MAPS OF BAROTROPIC TIDAL CURRENTS AS OBTAINED WITH THE OSU PREDICTION SOFTWARE FOR THE WORLD OCEAN AND THE MEDITERRANEAN SEA

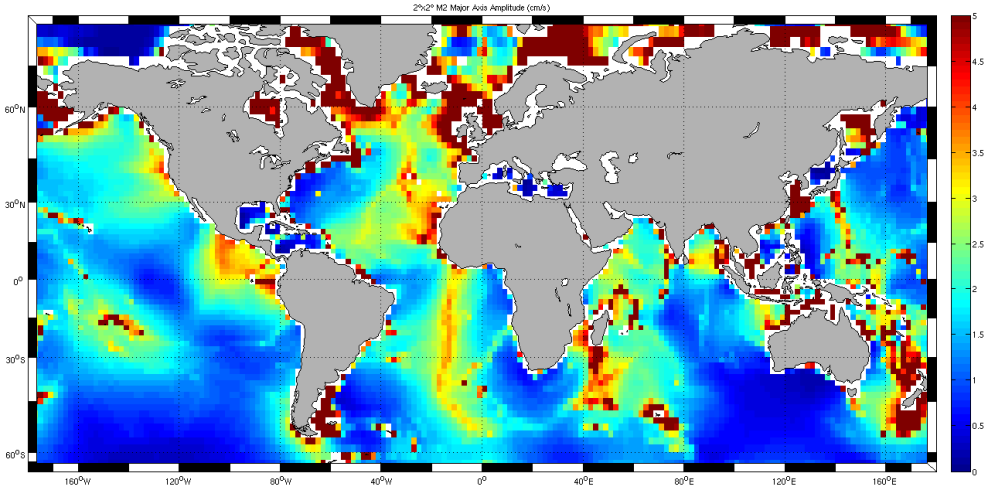

Thomas Miraglio[1] and Pierre-Marie Poulain

Istituto Nazionale di Oceanografia e di Geofisica Sperimentale (OGS),
Trieste, Italy

Approved for release by: ……

Dr. Paola Del Negro
Director, Oceanography Section

[1]also at ENSTA, Paris, France

TABLE of CONTENTS

1. Introduction

Several global ocean models, constrained by altimetry or not, are able to simulate quite accurately the barotropic tidal signal in sea level height (see for instance Kantha, 1995; Ray, 2001; Egbert and Ray, 2003; Stammer et al., 2014). The simulation of global barotropic tidal currents, however, appears less successful and also more difficult to compare with (or validate) with observations because the latter are relatively scarse and the barotropic component is not easy to estimate. With the goal of comparing modeled barotropic tidal currents with observations derived from surface drifters, the results obtained from the readily available Oregon State University (OSU) Tidal Prediction Software are presented in this report in the form of geographical maps of properties related to the barotropic tidal currents (amplitude of semi-major axis, ellipse inclination, rotary coefficient, Greenwich phase) for selected primary tidal constituents/frequencies for both the World Ocean and the Mediterranean Sea. Some details about OSU Tidal Prediction Software are presented in Section 2. Section 3 includes the results for the modeled barotropic tidal currents over the World Ocean, whereas the same results for the Mediterranean Sea are presented in Section 4. Conclusions are included in Section5.

2. The OSU barotropic tide model

Global and regional inverse solutions were provided by the OSU Tidal Prediction Software (OTPS) and its matlab package. These solutions are based on barotropic inverse tidal solutions obtained with the OSU Tidal Inversion Software (OTIS). The methods used to compute the tidal model are described in details by Egbert et al. (1994) and Egbert and Erofeeva (2002). The results for the global solution were extracted from TPXO7.2, a 1/4º × 1/4 º model which best-fits, in a least-squares sense, the Laplace Tidal Equations and along track averaged data from TOPEX/Poseidon and Jason (on TOPEX/POSEIDON tracks since 2002) obtained with OTIS. The regional Mediterranean solution was extracted from the 1/30 º × 1/30 º regional solution provided on the OTIS website. It uses data from 531 Topex Poseidon cycles (all available data) ; 114 Topex Tandem cycles (all available data), and 20000 ERS data sites (for M2 and K1 only). The barotropic tidal currents were considered for the eight primary (M2, S2, N2, K2, K1, O1, P1, Q1) harmonic constituents.

In order to provide gridded fields of simulated barotropic tidal currents with spatial smoothing comparable to the tidal products obtained from drifter data, the model results were averaged in 2º × 2 º and 1º × 1 º for the World Ocean and Mediterranean Sea, respectively. Special care was taken in the averages in the vicinity of coasts (NaN values were excluded) and also when averaging angles were near zero degree (eastward direction).

3. Barotropic tidal currents in the World Ocean

The following figures (Figs. 1 to 8) illustrate the geographical distribution of the barotropic tidal currents as obtained from OTIS for the eight primary tidal constituents (semi-diurnal frequencies: M2, S2, N2, K2; and diurnal frequencies: K1, O1, P1, Q1) in the World Ocean. The following parameters are shown in color-coded contour plots: the amplitude of the semi-major axis, the ellipse inclination, the rotary coefficient and the Greenwich phase. The rotary coefficient varies between -1 and 1 and positive (negative) values correspond to CW (CCW) sense of rotation. Rectilinear reversing tidal currents have a rotary coefficient equal to zero. By definition, the Greenwich phase is zero when the tidal constituent is maximal (velocity vector aligned with major axis of tidal ellipse) at the Greenwich meridian. The inclination is given in degrees counterclockwise from East.

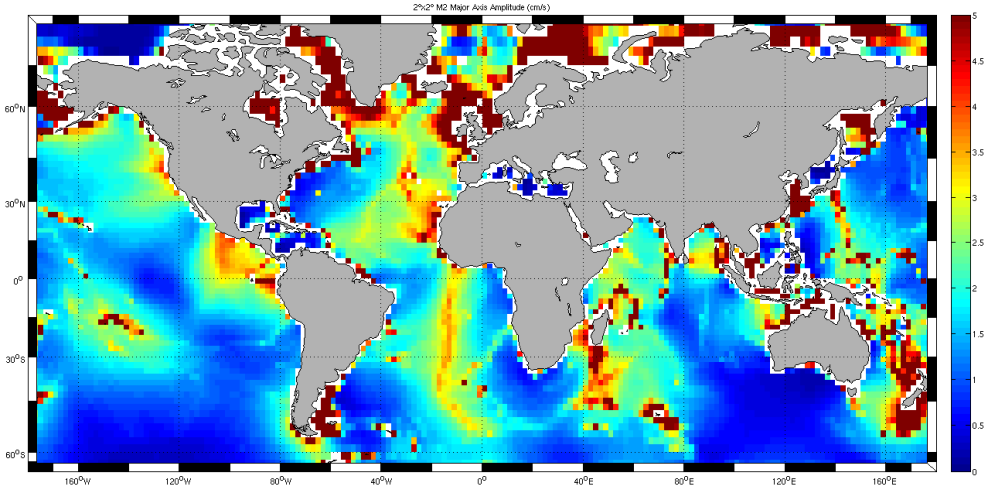
2°x2° M2 Major Axis Amplitude (cm/s)
60°N
30°N
0°
30°S
60°S
160°W
120°W
80°W
40°W
0°
40°E
80°E
120°E
160°E
5
4.5
4
3.5
3
2.5
2
1.5
1
0.5
0

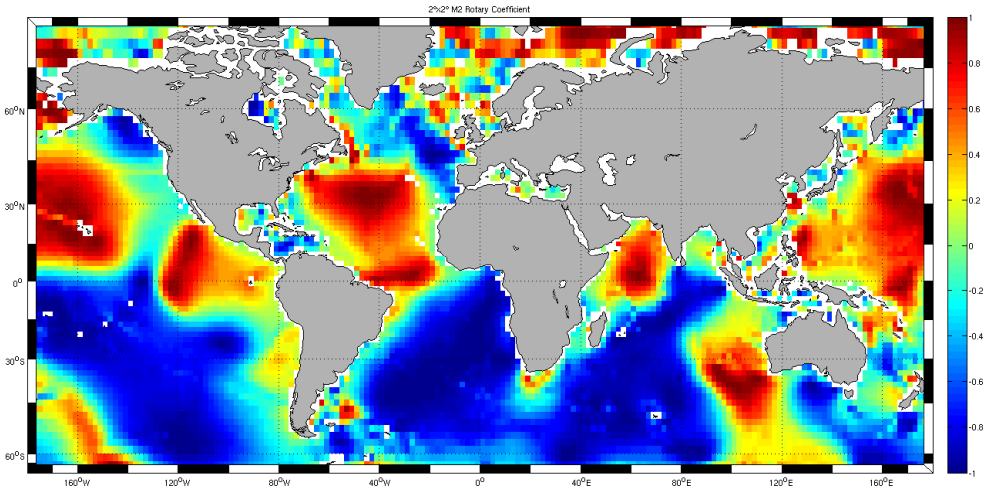
2°x2° M2 Rotary Coefficient
60°N
30°N
0°
30°S
60°S
160°W
120°W
80°W
40°W
0°
40°E
80°E
120°E
160°E
1
0.8
0.6
0.4
0.2
0
-0.2
-0.4
-0.6
-0.8
-1

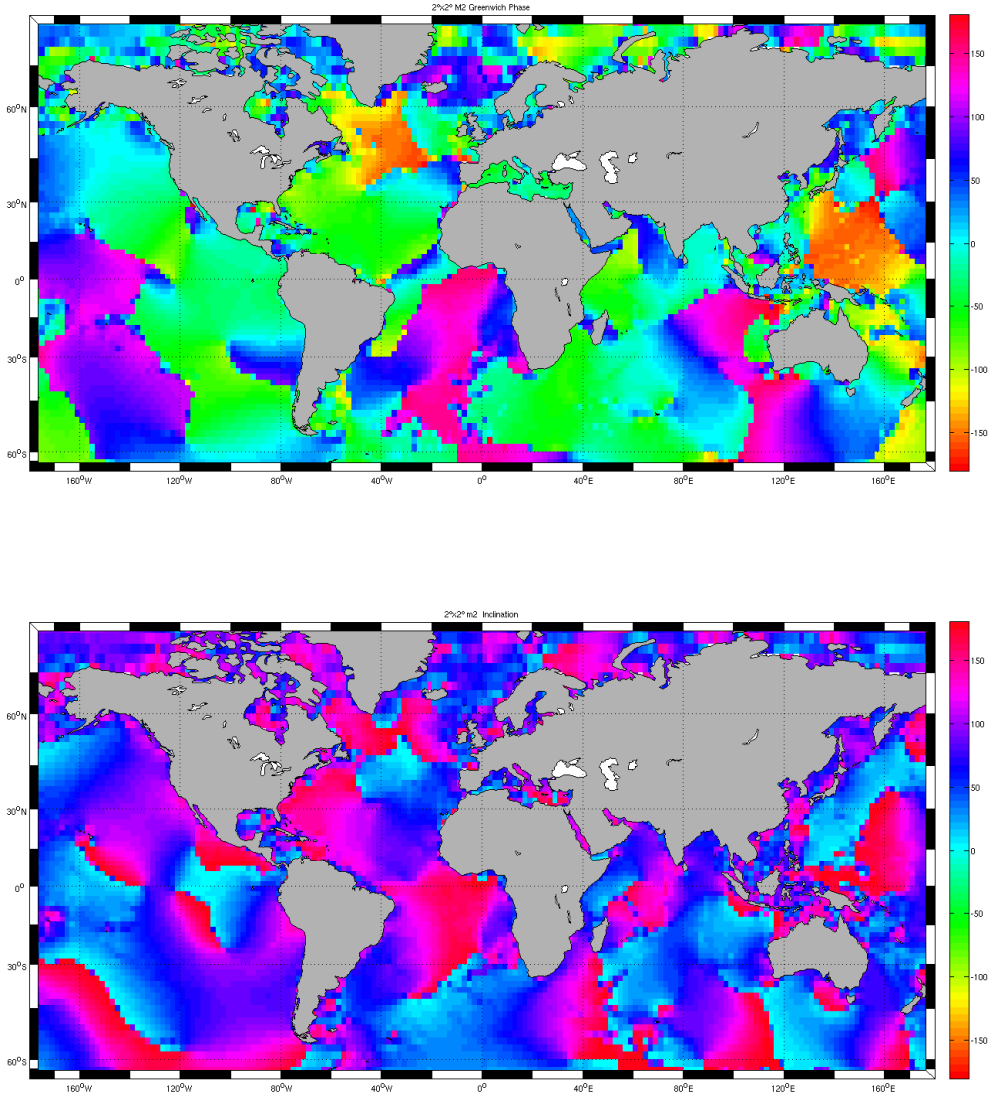

Figure 1. Amplitude of semi-major axis, rotary coefficient, Greenwich phase and ellipse inclination of M2 tidal currents averaged in 2º x 2º bins. Amplitudes in excess of 5 cm/s are saturated. Maximal amplitude of 99 cm/s occurs in the Yellow Sea.

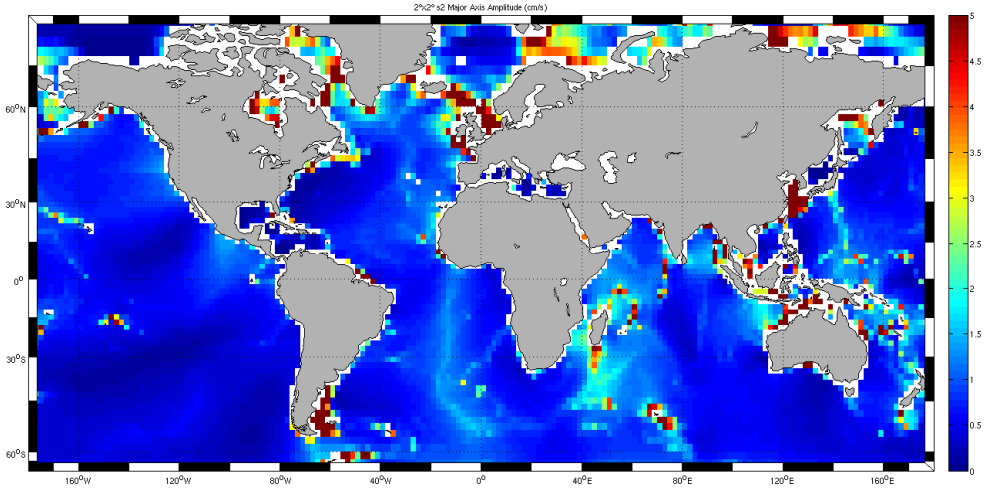
2°x2° s2 Major Axis Amplitude (cm/s)
60°N
30°N
0°
30°S
60°S
160°W
120°W
80°W
40°W
0°
40°E
80°E
120°E
160°E
5
4.5
4
3.5
3
2.5
2
1.5
1
0.5
0

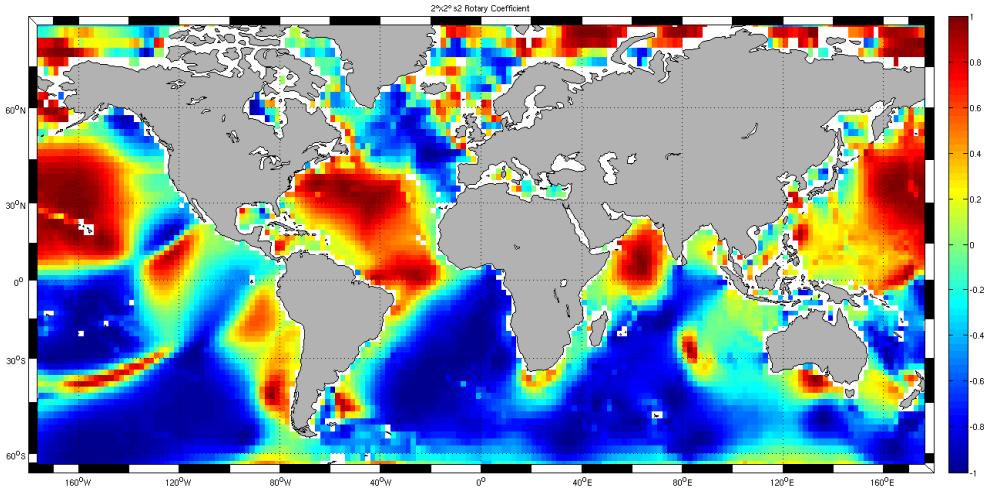
2°x2° s2 Rotary Coefficient
60°N
30°N
0°
30°S
60°S
160°W
120°W
80°W
40°W
0°
40°E
80°E
120°E
160°E
1
0.8
0.6
0.4
0.2
0
-0.2
-0.4
-0.6
-0.8
-1

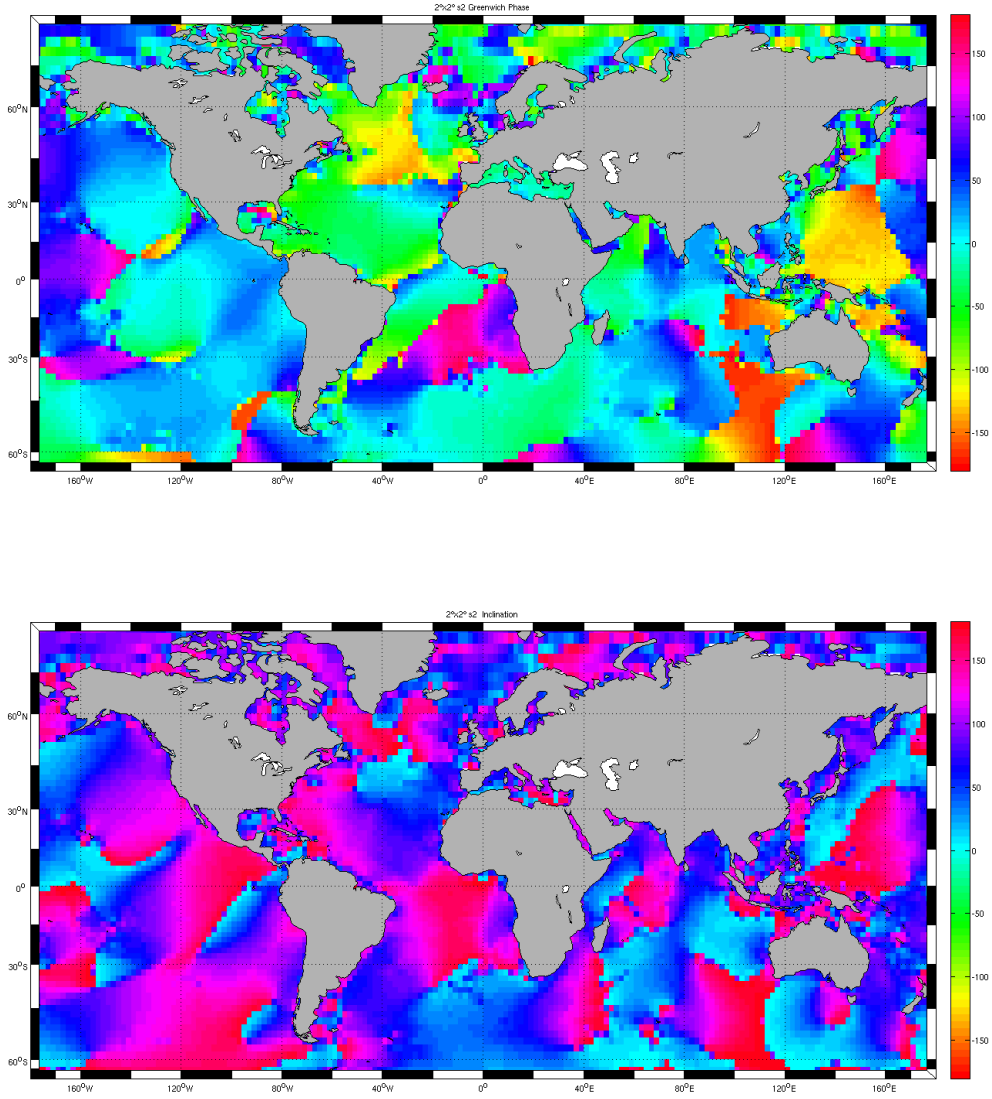

Figure 2. Same as in Figure 1 but for S2 tidal currents. Maximal amplitude of 34 cm/s occurs in Hudson Strait (Canada).

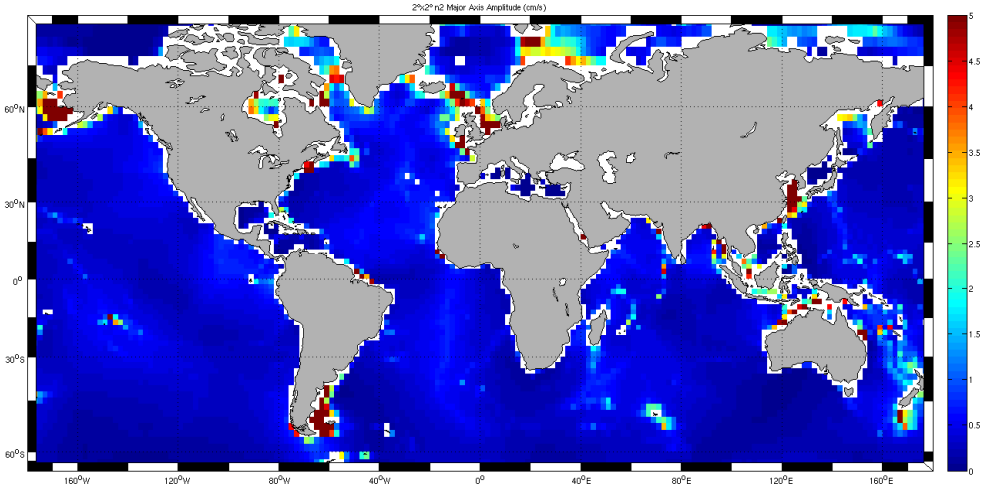
2°x2° n2 Major Axis Amplitude (cm/s)
60°N
30°N
0°
30°S
60°S
160°W
120°W
80°W
40°W
0°
40°E
80°E
120°E
160°E
5
4.5
4
3.5
3
2.5
2
1.5
1
0.5
0

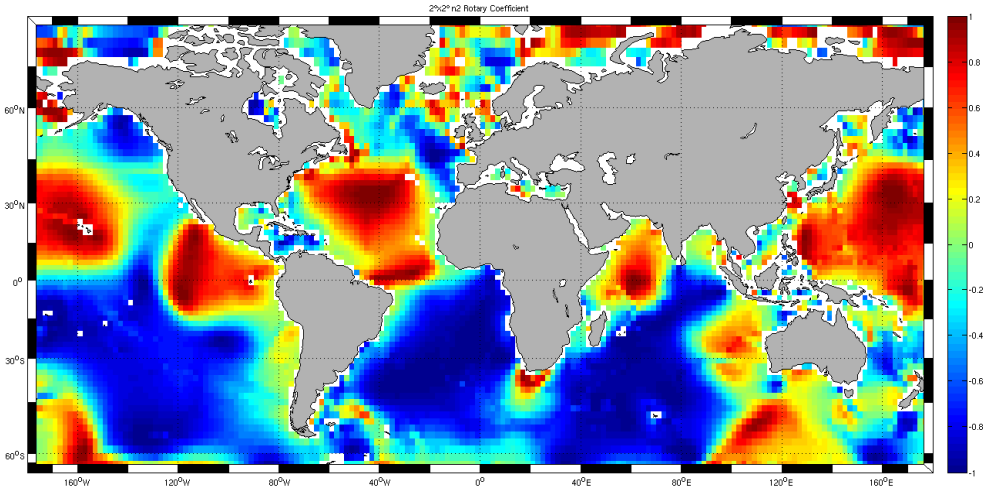
2°x2° n2 Rotary Coefficient
60°N
30°N
0°
30°S
60°S
160°W
120°W
80°W
40°W
0°
40°E
80°E
120°E
160°E
1
0.8
0.6
0.4
0.2
0
-0.2
-0.4
-0.6
-0.8
-1

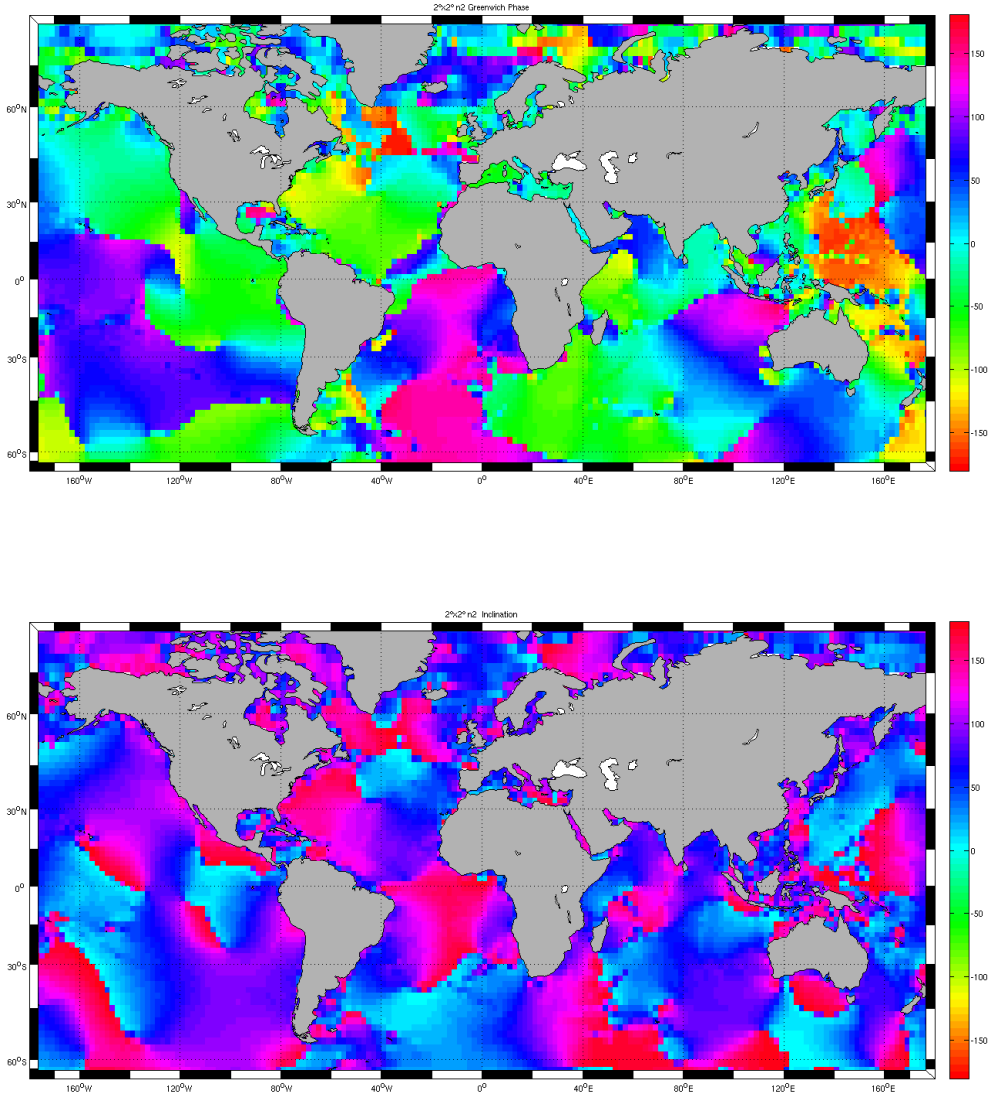

Figure 3. Same as in Figure 1 but for N2 tidal currents. Maximal amplitude of 19 cm/s occurs in Hudson Strait (Canada).

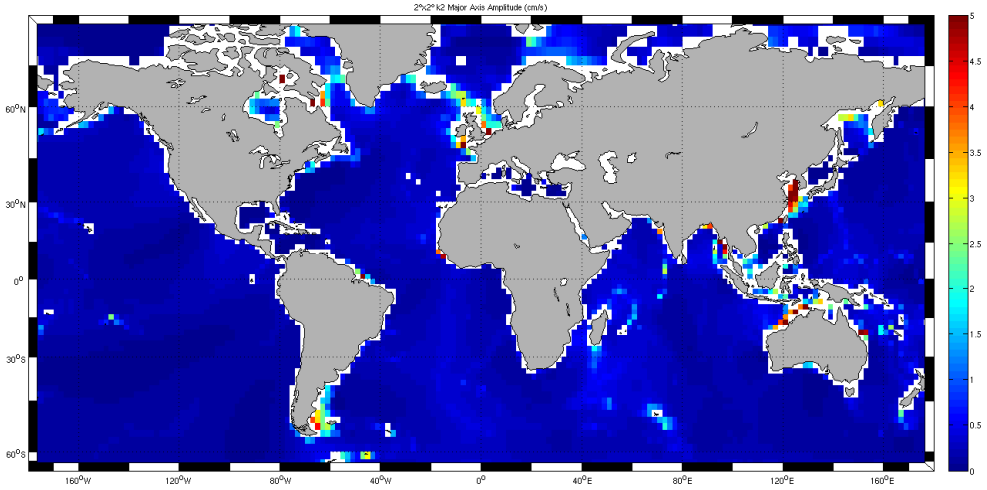
2°x2° k2 Major Axis Amplitude (cm/s)
60°N
30°N
0°
30°S
60°S
160°W
120°W
80°W
40°W
0°
40°E
80°E
120°E
160°E
5
4.5
4
3.5
3
2.5
2
1.5
1
0.5
0

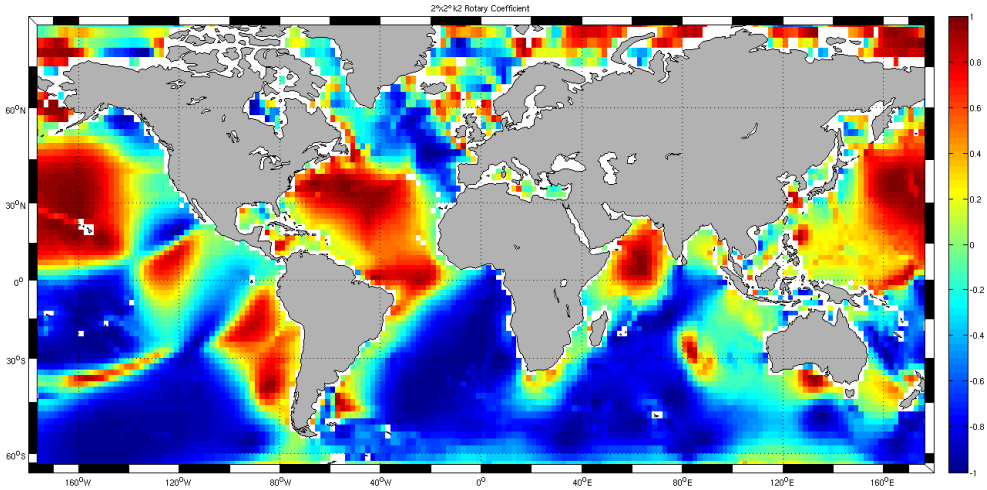
2°x2° k2 Rotary Coefficient
60°N
30°N
0°
30°S
60°S
160°W
120°W
80°W
40°W
0°
40°E
80°E
120°E
160°E
1
0.8
0.6
0.4
0.2
0
-0.2
-0.4
-0.6
-0.8
-1

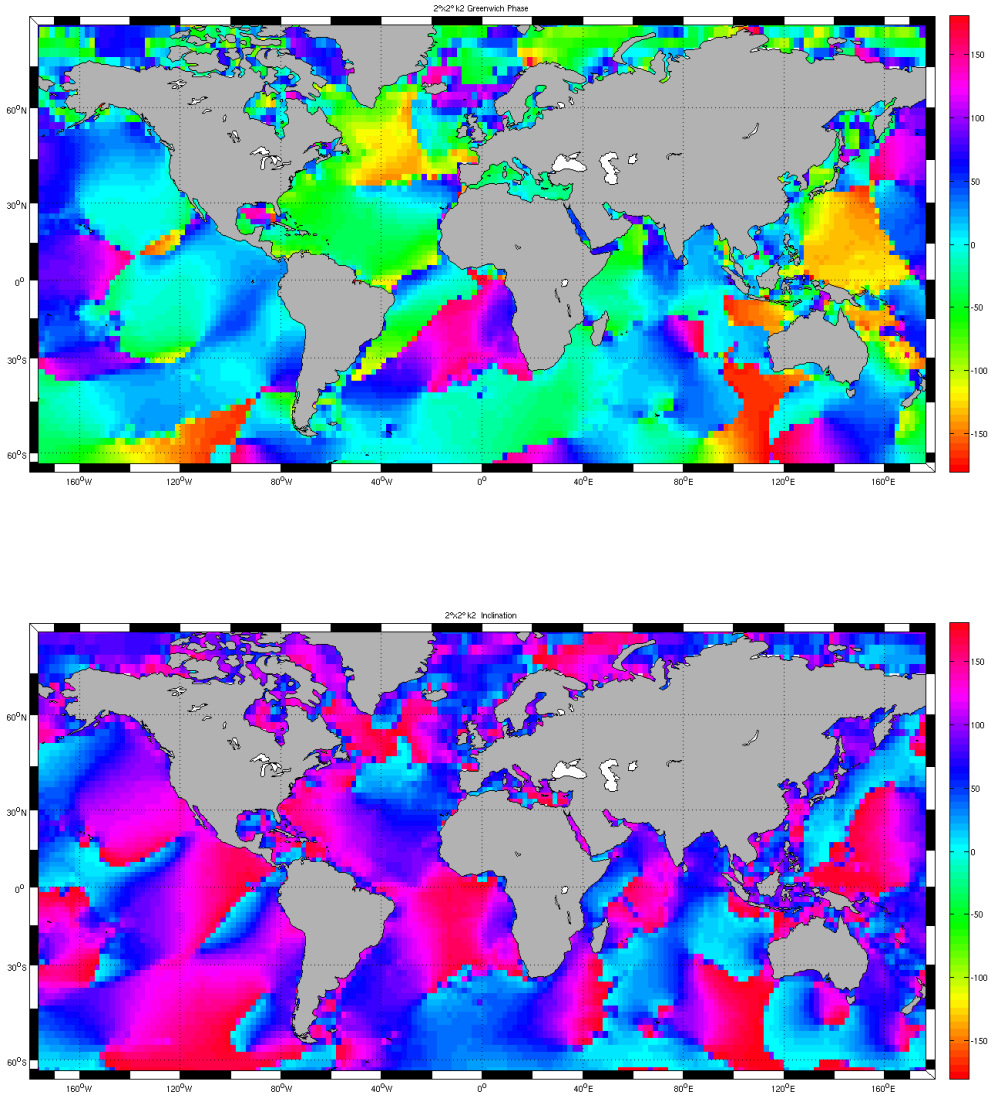

Figure 4. Same as in Figure 1 but for K2 tidal currents. Maximal amplitude of 10 cm/s occurs in Hudson Strait (Canada).

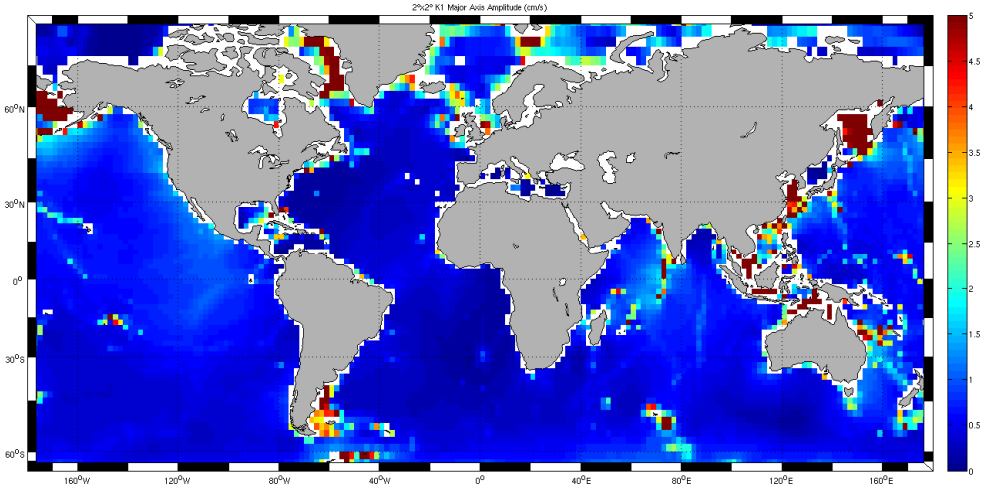
2°x2° K1 Major Axis Amplitude (cm/s)
60°N
30°N
0°
30°S
60°S
160°W
120°W
80°W
40°W
0°
40°E
80°E
120°E
160°E
5
4.5
4
3.5
3
2.5
2
1.5
1
0.5
0

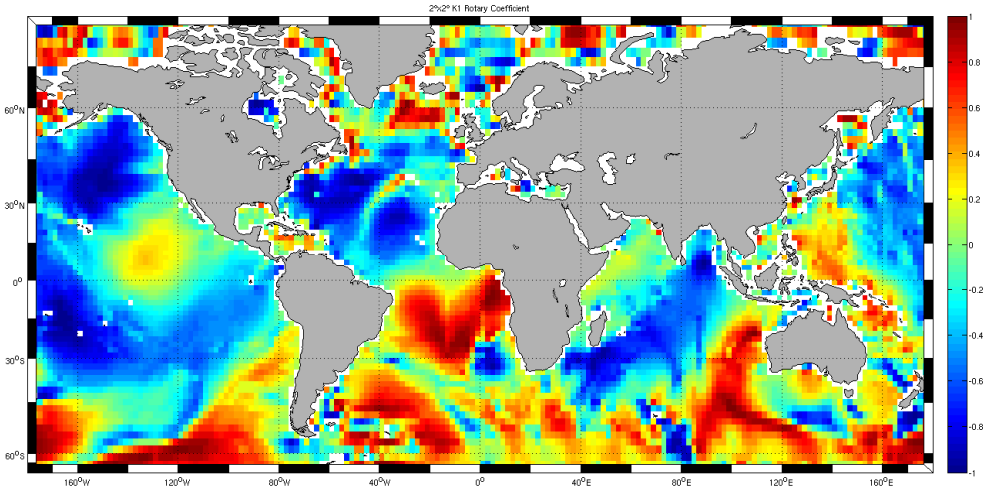
2°x2° K1 Rotary Coefficient
60°N
30°N
0°
30°S
60°S
160°W
120°W
80°W
40°W
0°
40°E
80°E
120°E
160°E
1
0.8
0.6
0.4
0.2
0
-0.2
-0.4
-0.6
-0.8
-1

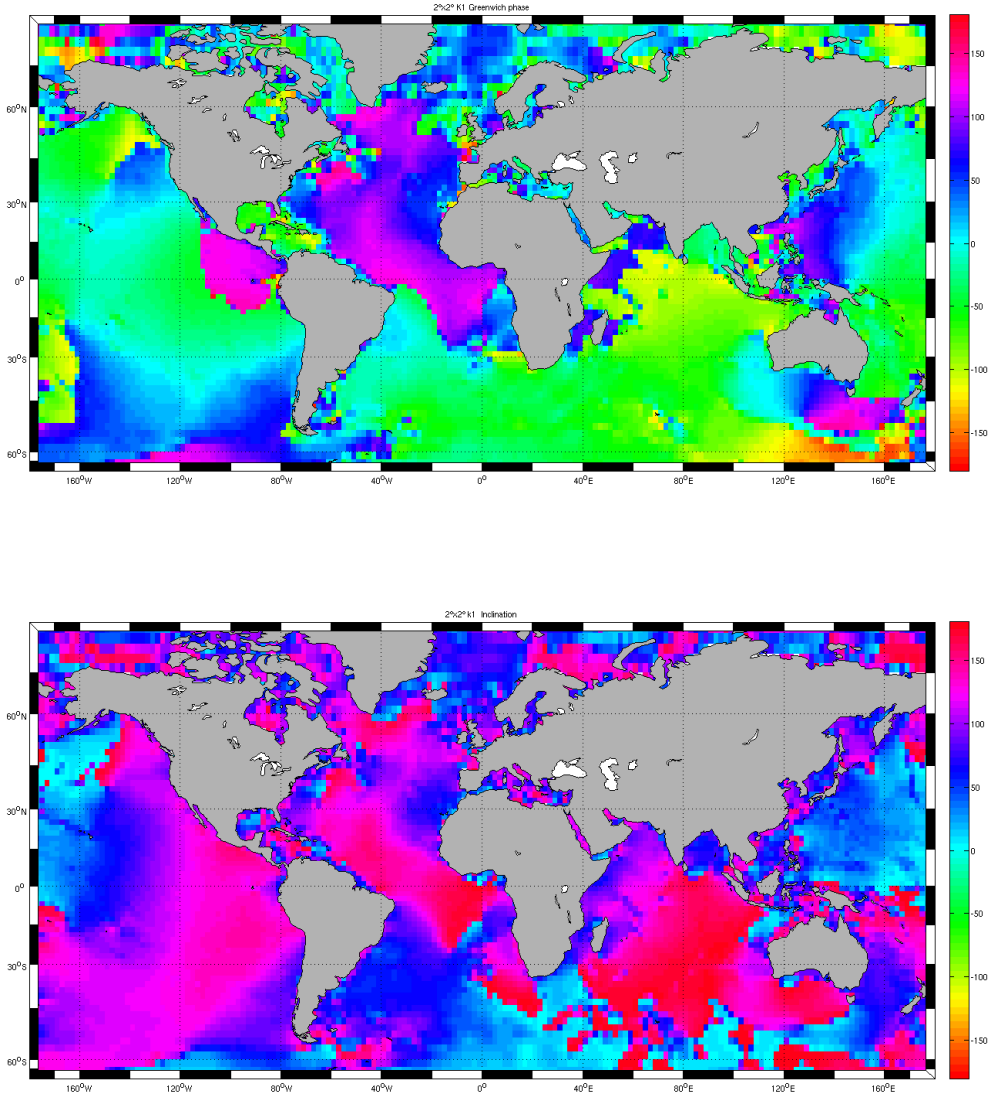

Figure 5. Same as in Figure 1 but for K1 tidal currents. Maximal amplitude of 57 cm/s occurs in Ross Sea (not shown).

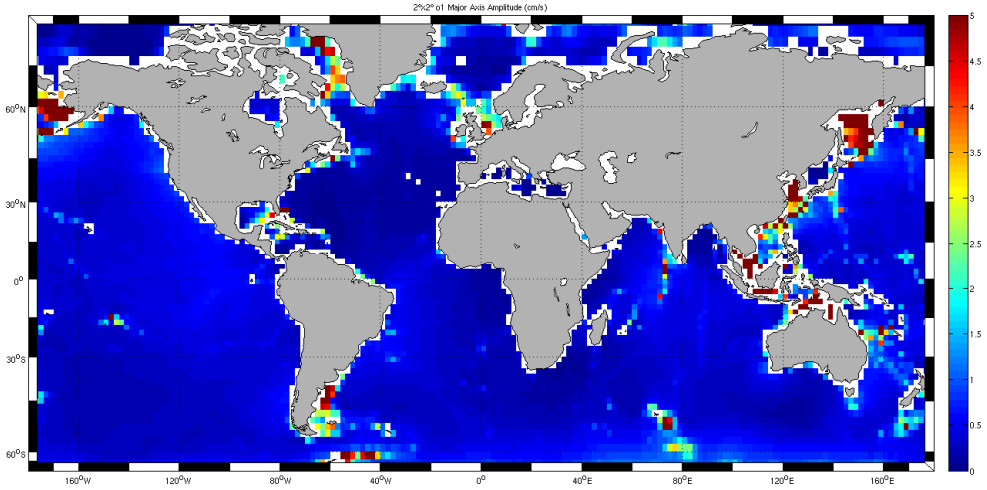
2°x2° o1 Major Axis Amplitude (cm/s)
60°N
30°N
0°
30°S
60°S
160°W
120°W
80°W
40°W
0°
40°E
80°E
120°E
160°E
5
4.5
4
3.5
3
2.5
2
1.5
1
0.5
0

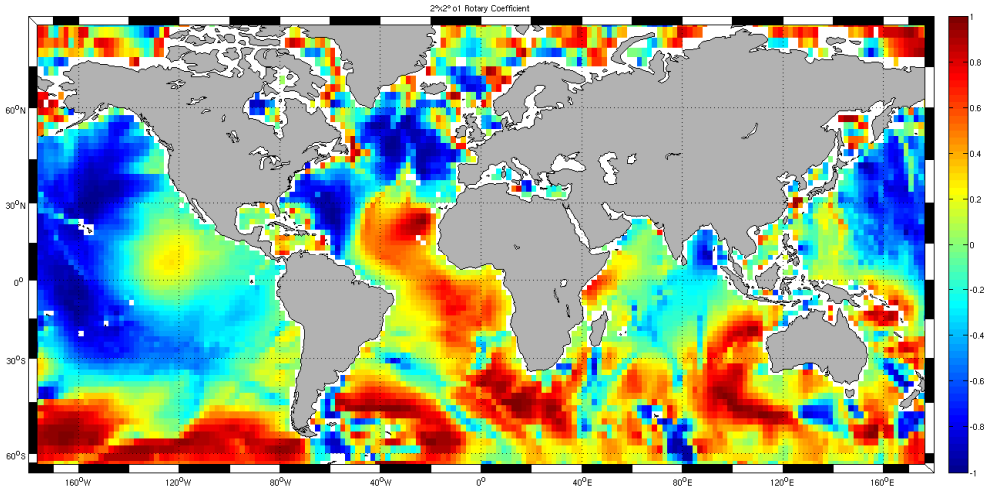
2°x2° o1 Rotary Coefficient
60°N
30°N
0°
30°S
60°S
160°W
120°W
80°W
40°W
0°
40°E
80°E
120°E
160°E
1
0.8
0.6
0.4
0.2
0
-0.2
-0.4
-0.6
-0.8
-1

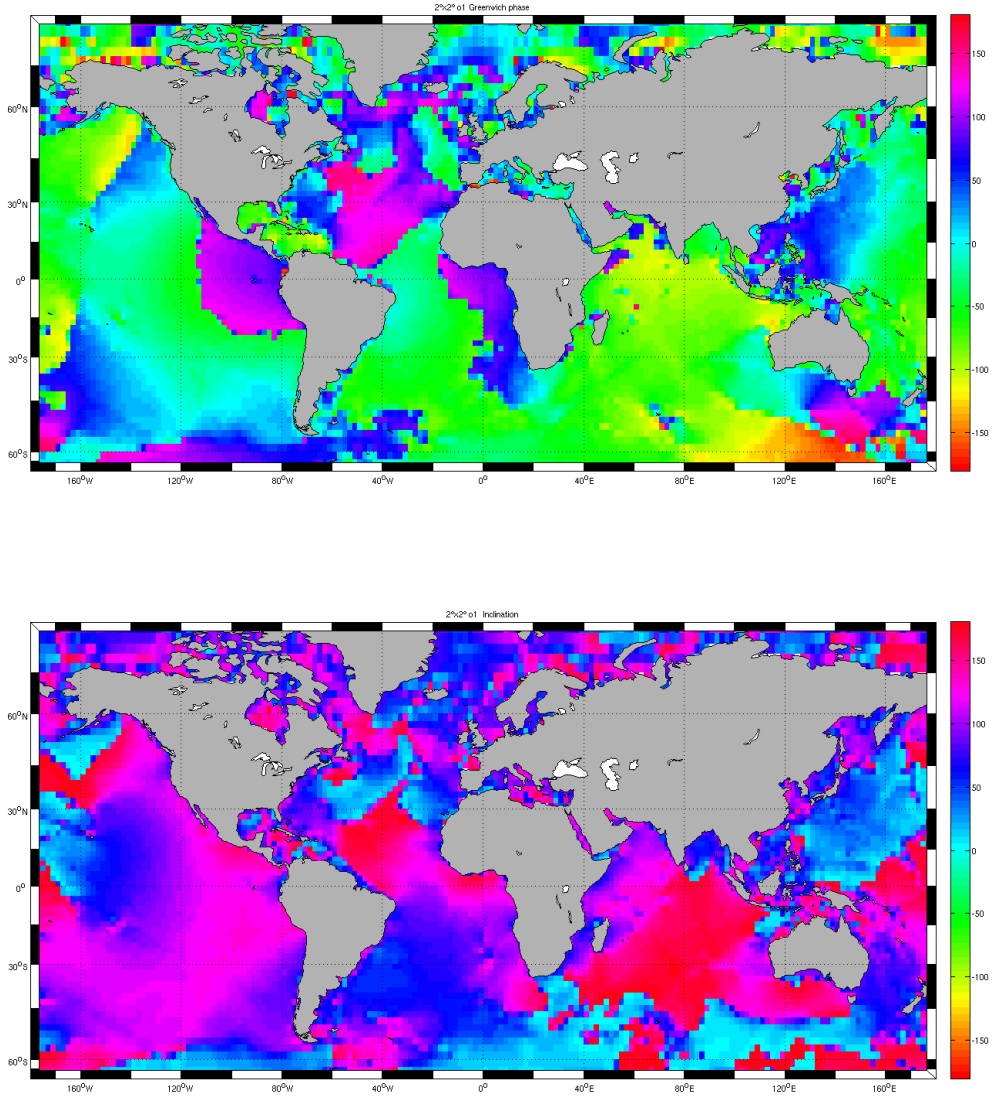

Figure 6. Same as in Figure 1 but for O1 tidal currents. Maximal amplitude of 29 cm/s occurs in the Indonesian Sea.

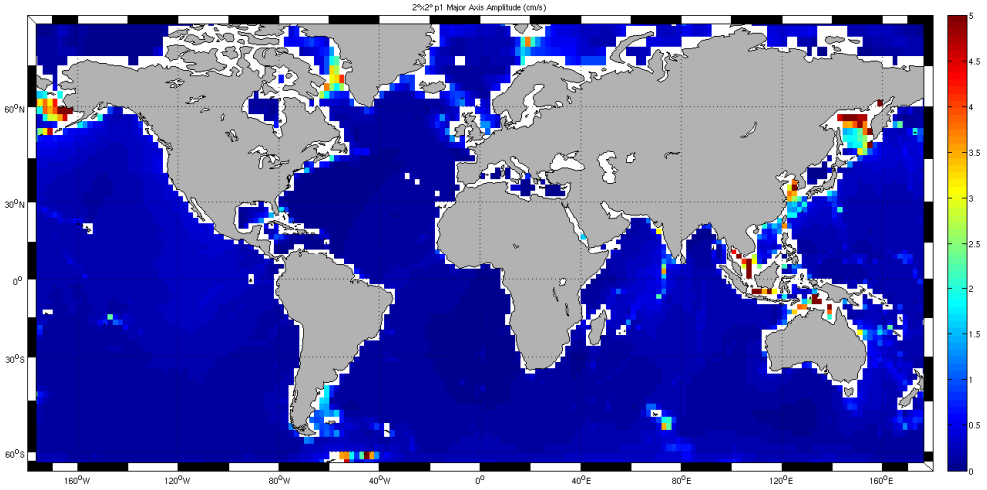
2°x2° p1 Major Axis Amplitude (cm/s)
60°N
30°N
0°
30°S
60°S
160°W
120°W
80°W
40°W
0°
40°E
80°E
120°E
160°E
5
4.5
4
3.5
3
2.5
2
1.5
1
0.5
0

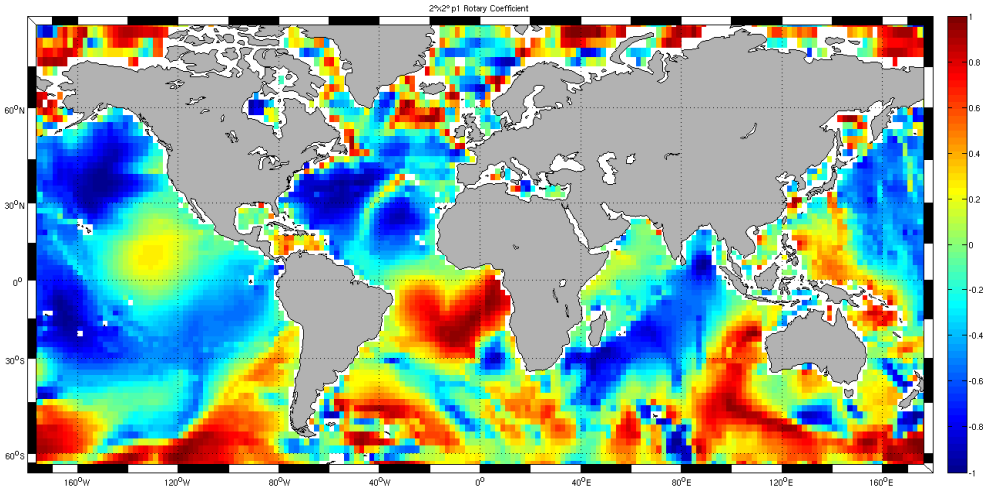
2°x2° p1 Rotary Coefficient
60°N
30°N
0°
30°S
60°S
160°W
120°W
80°W
40°W
0°
40°E
80°E
120°E
160°E
1
0.8
0.6
0.4
0.2
0
-0.2
-0.4
-0.6
-0.8
-1

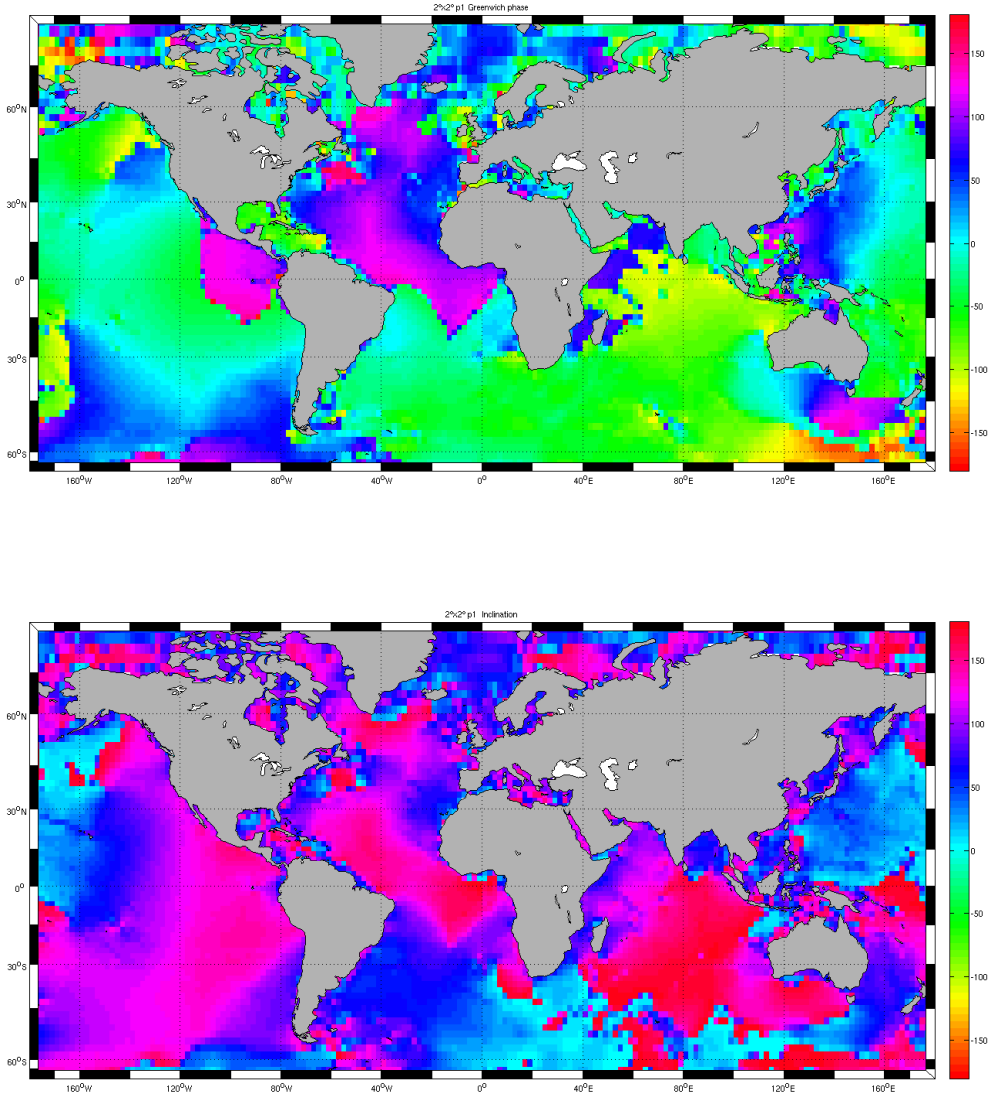

Figure 7. Same as in Figure 1 but for P1 tidal currents. Maximal amplitude of 13 cm/s occurs in Ross Sea (not shown).

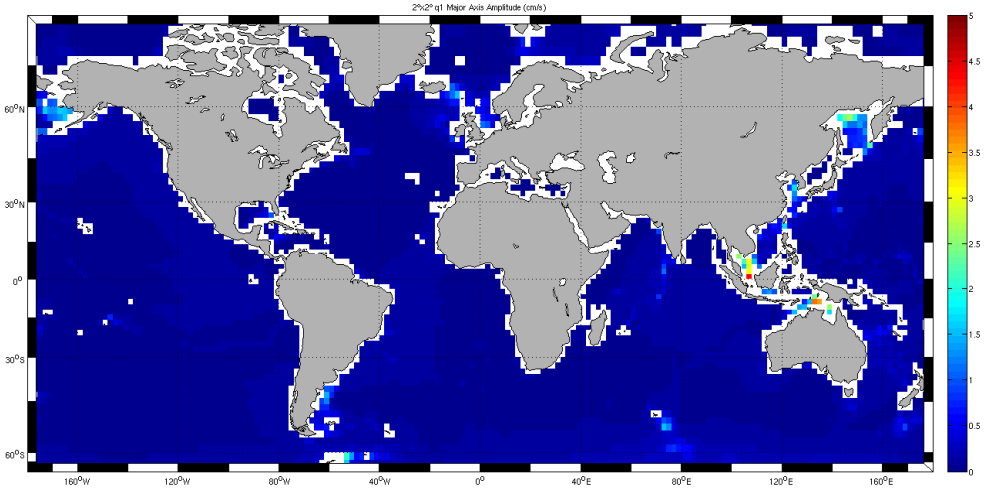
2°x2° q1 Major Axis Amplitude (cm/s)
60°N
30°N
0°
30°S
60°S
160°W
120°W
80°W
40°W
0°
40°E
80°E
120°E
160°E
5
4.5
4
3.5
3
2.5
2
1.5
1
0.5
0

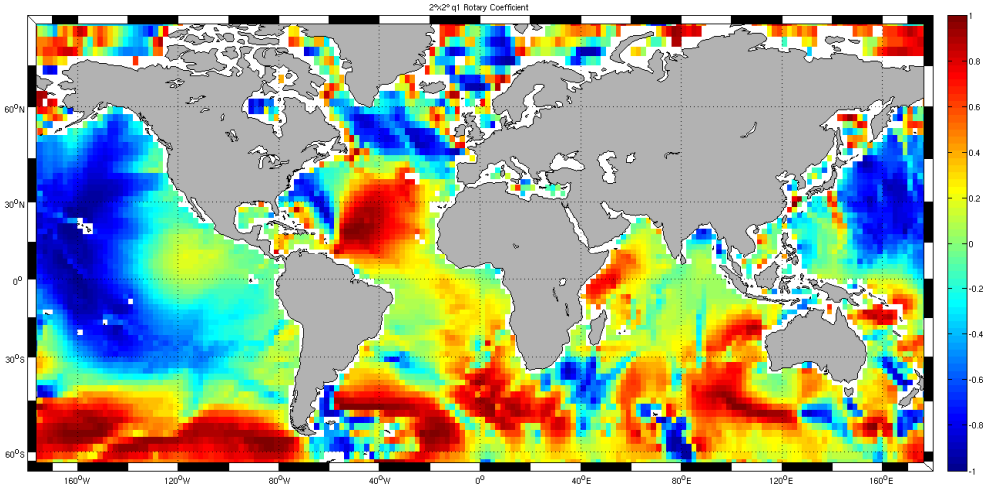
2°x2° q1 Rotary Coefficient
60°N
30°N
0°
30°S
60°S
160°W
120°W
80°W
40°W
0°
40°E
80°E
120°E
160°E
1
0.8
0.6
0.4
0.2
0
-0.2
-0.4
-0.6
-0.8
-1

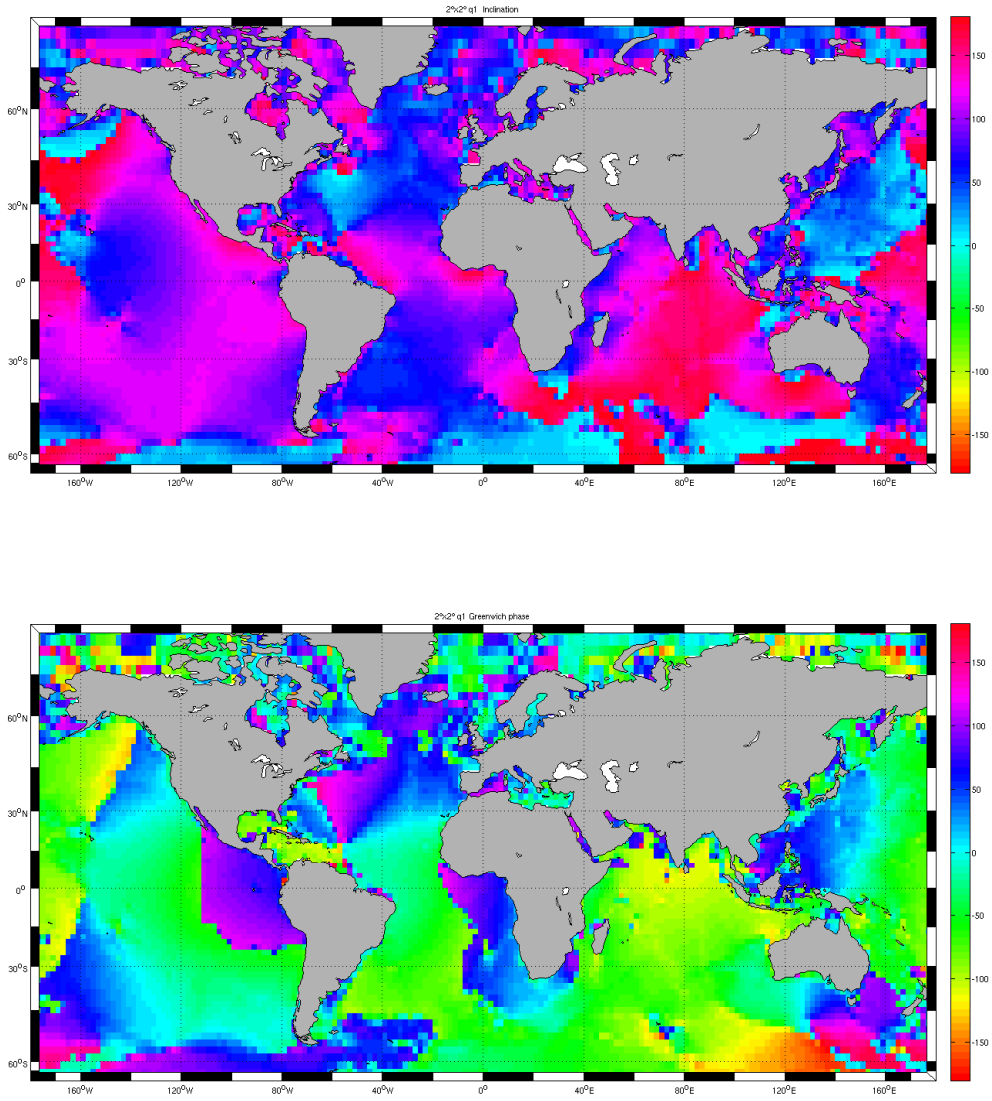

Figure 8. Same as in Figure 1 but for Q1 tidal currents. Maximal amplitude of 5 cm/s occurs in Ross Sea (not shown).

4. Barotropic tidal currents in the Mediterranean Sea

The following figures (Figs. 9 to 16) illustrate the geographical distribution of the barotropic tidal currents as obtained from OTIS for the eight primary tidal constituents in the Mediterranean Sea.

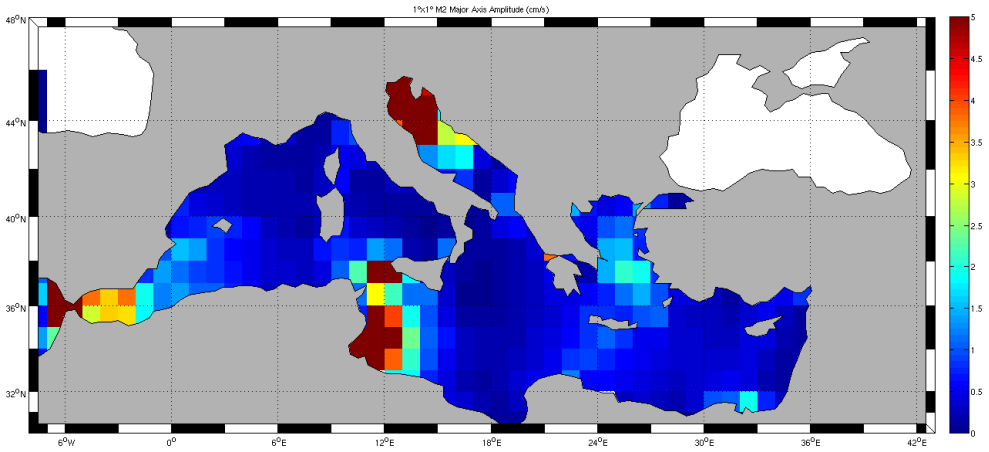

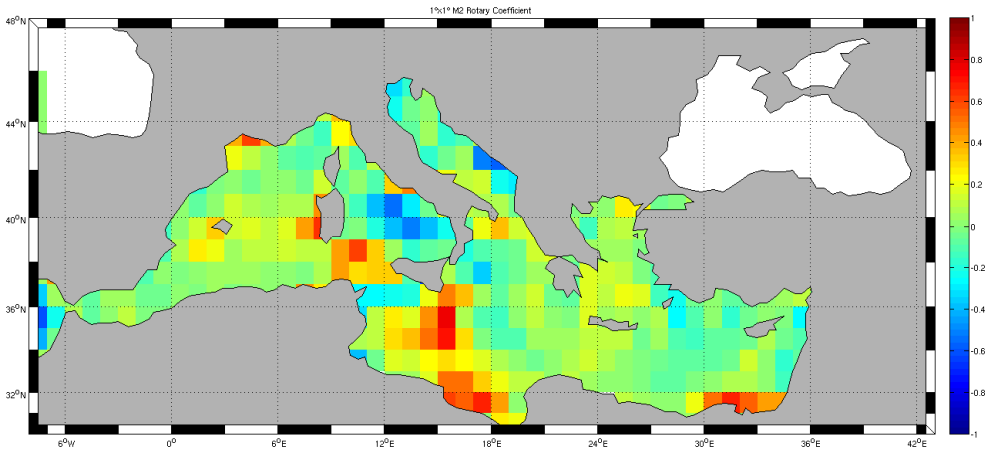

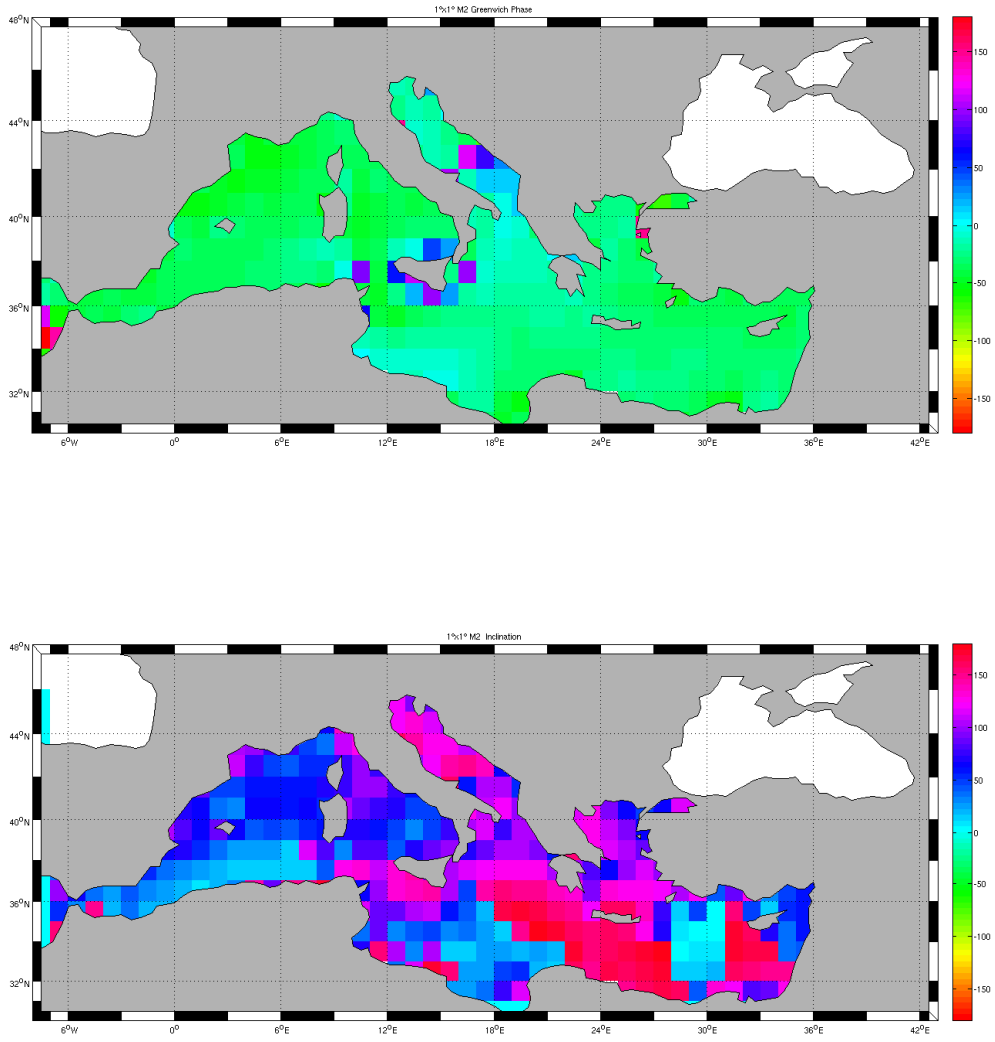

Figure 9. Amplitude of semi-major axis, rotary coefficient, Greenwich phase and ellipse inclination of M2 tidal currents averaged in 1º x 1º bin over the Mediterranean Sea. Amplitudes in excess of 5 cm/s are saturated. Maximal amplitude of 20 cm/s occurs near the Strait of Gibraltar.

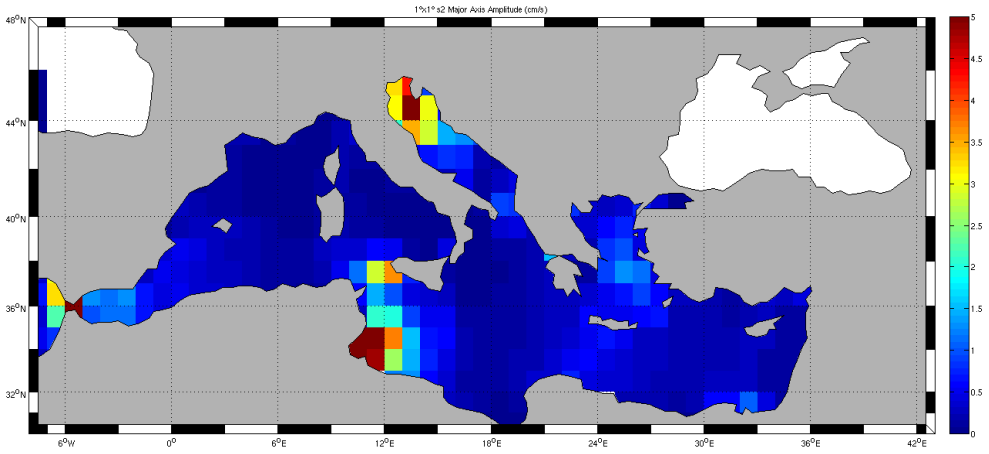
1°x1° s2 Major Axis Amplitude (cm/s)
48°N
44°N
40°N
36°N
32°N
6°W
0°
6°E
12°E
18°E
24°E
30°E
36°E
42°E
5
4.5
4
3.5
3
2.5
2
1.5
1
0.5
0

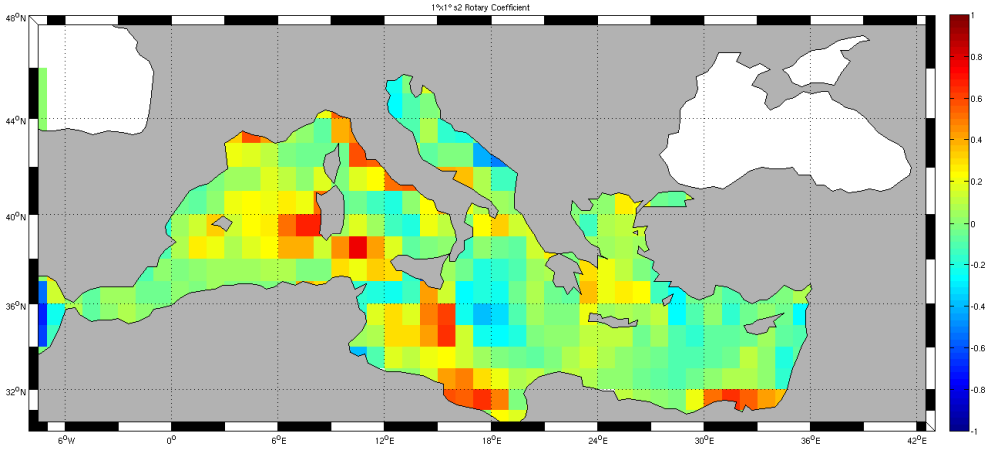
1°x1° s2 Rotary Coefficient
48°N
44°N
40°N
36°N
32°N
6°W
0°
6°E
12°E
18°E
24°E
30°E
36°E
42°E
1
0.8
0.6
0.4
0.2
0
-0.2
-0.4
-0.6
-0.8
-1

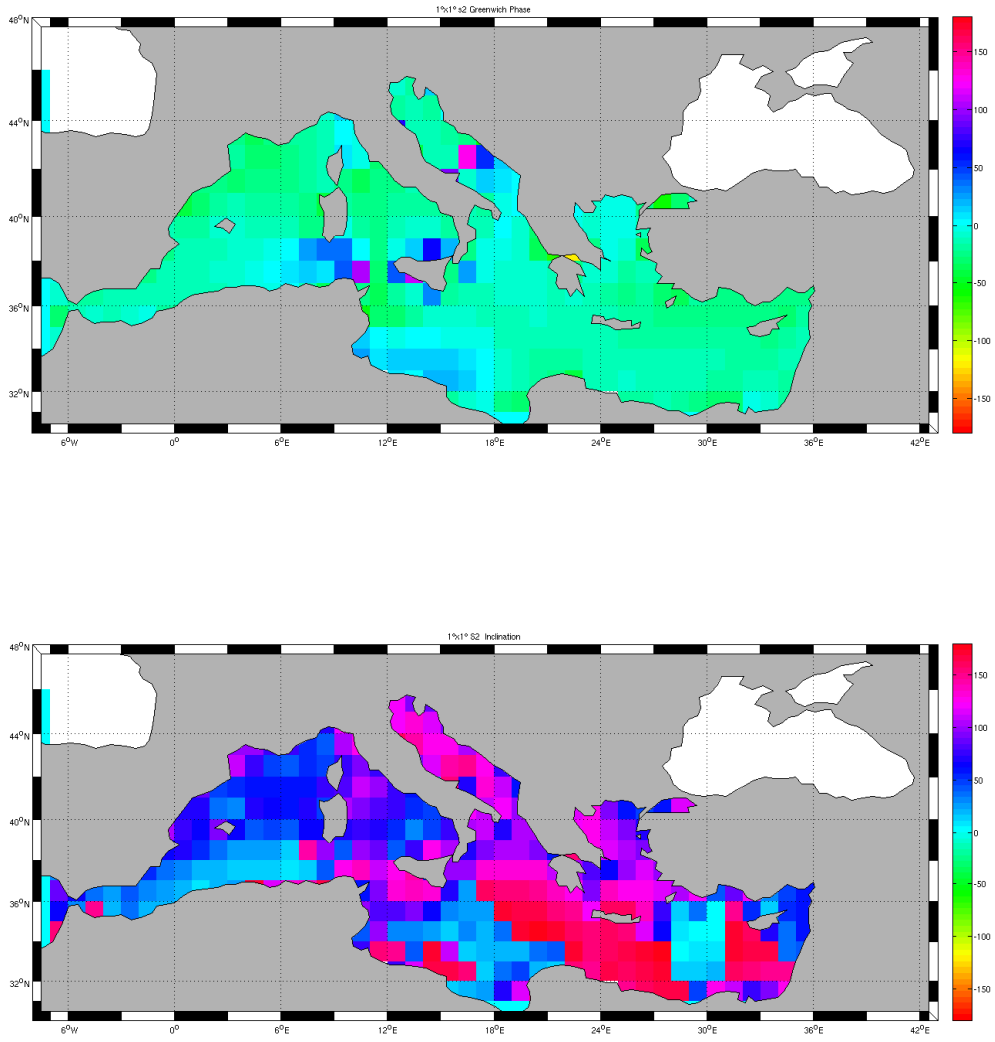

Figure 10. Same as in Figure 9 but for S2 tidal currents. Maximal amplitude of 10 cm/s occurs in the Gulf of Gabes.

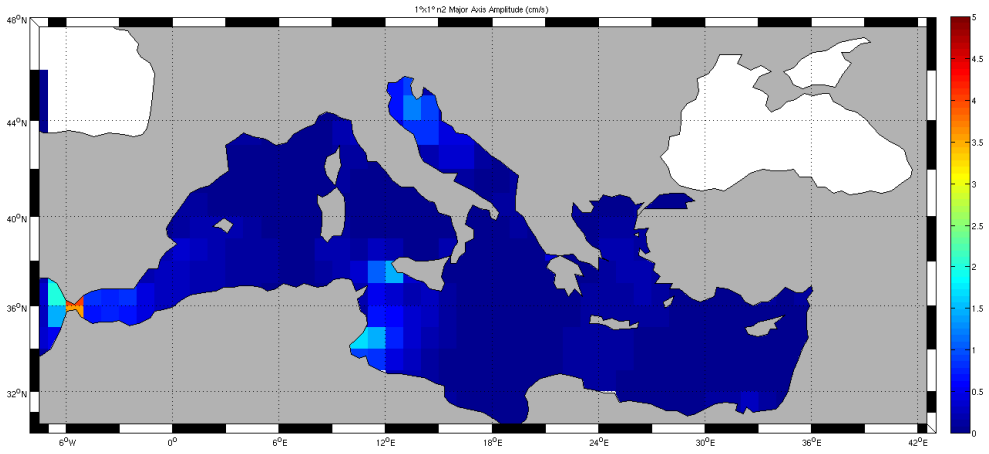
1°x1°n2 Major Axis Amplitude (cm/s)
46°N
44°N
40°N
36°N
32°N
6°W
0°
6°E
12°E
18°E
24°E
30°E
36°E
42°E
5
4.5
4
3.5
3
2.5
2
1.5
1
0.5
0

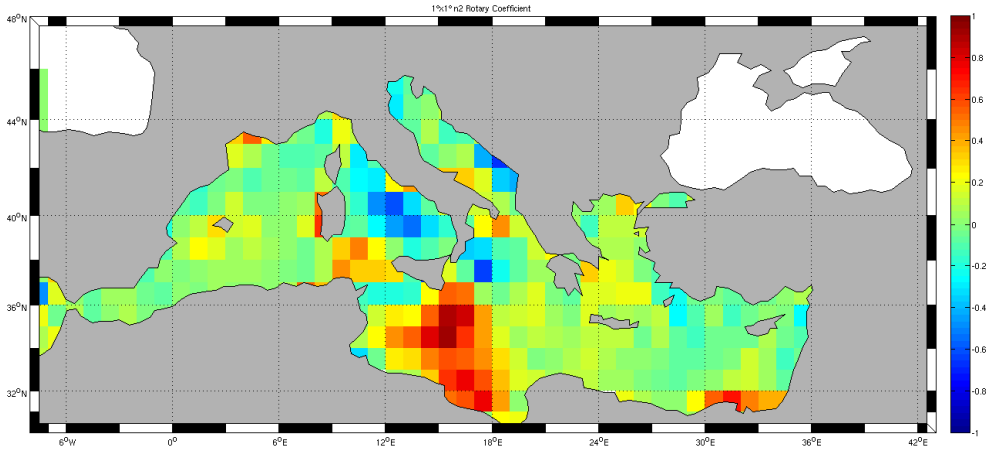
1°x1°n2 Rotary Coefficient
46°N
44°N
40°N
36°N
32°N
6°W
0°
6°E
12°E
18°E
24°E
30°E
36°E
42°E
1
0.8
0.6
0.4
0.2
0
-0.2
-0.4
-0.6
-0.8
-1

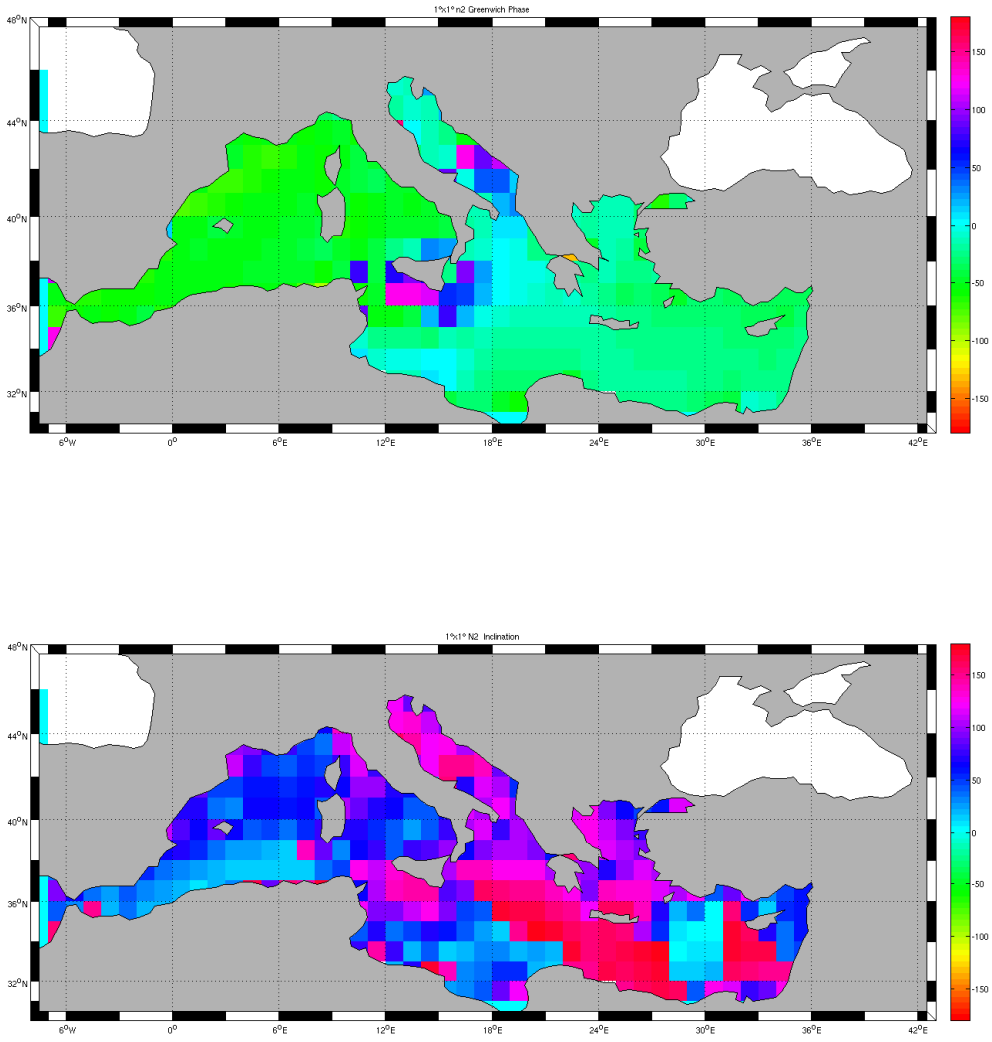

Figure 11. Same as in Figure 9 but for N2 tidal currents. Maximal amplitude of 4 cm/s occurs near the Strait of Gibraltar.

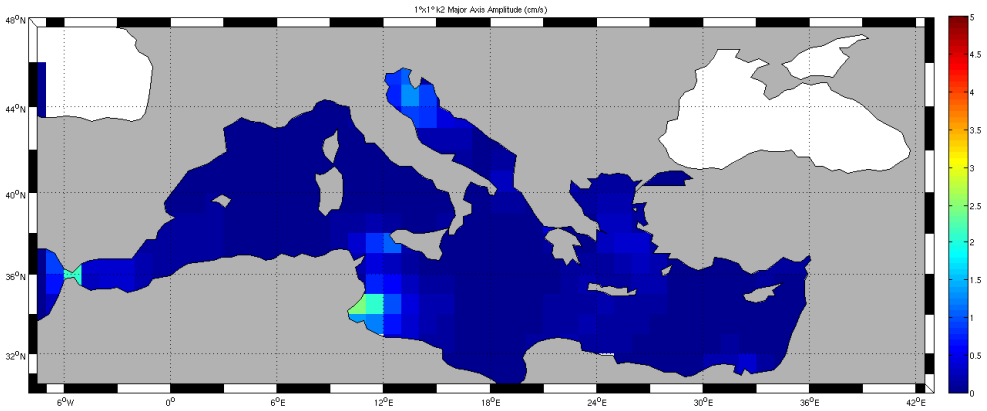
1°x1°k2 Major Axis Amplitude (cm/s)
48°N
44°N
40°N
36°N
32°N
6°W
0°
6°E
12°E
18°E
24°E
30°E
36°E
42°E
5
4.5
4
3.5
3
2.5
2
1.5
1
0.5
0

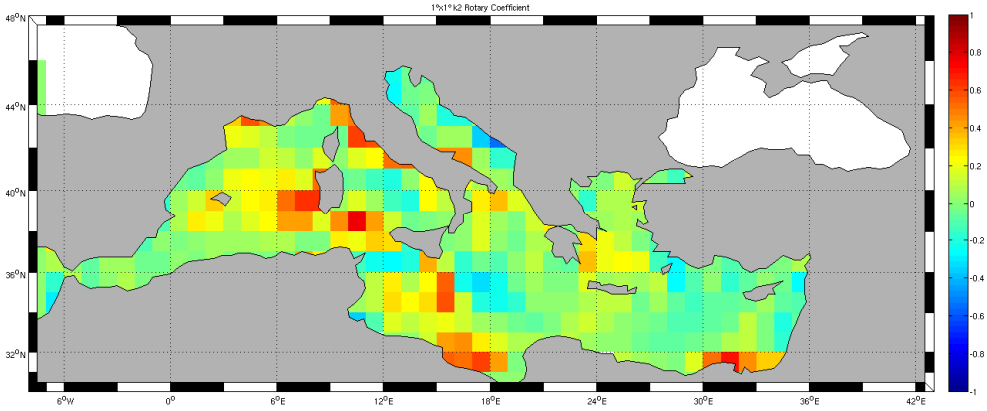
1°x1°k2 Rotary Coefficient
48°N
44°N
40°N
36°N
32°N
6°W
0°
6°E
12°E
18°E
24°E
30°E
36°E
42°E
1
0.8
0.6
0.4
0.2
0
-0.2
-0.4
-0.6
-0.8
-1

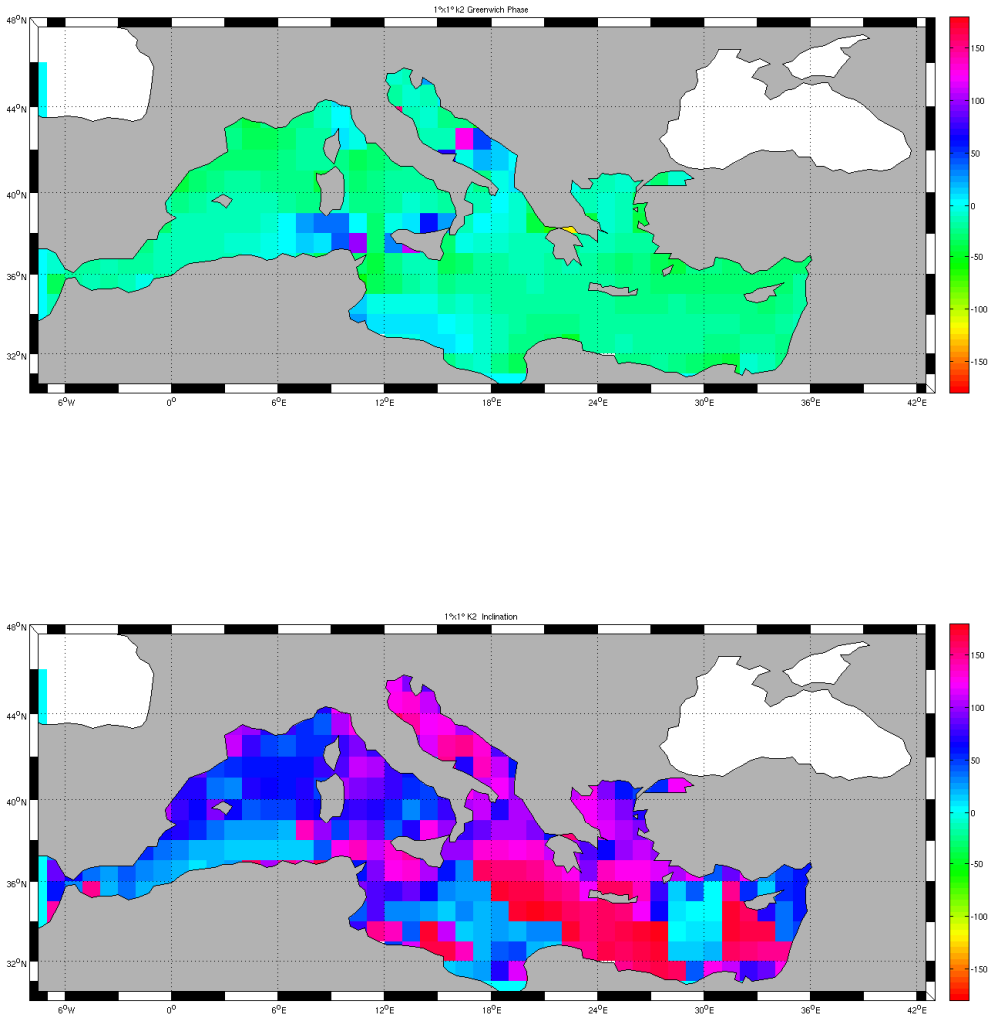

Figure 12. Same as in Figure 9 but for K2 tidal currents. Maximal amplitude of 2 cm/s occurs in the Gulf of Gabes.

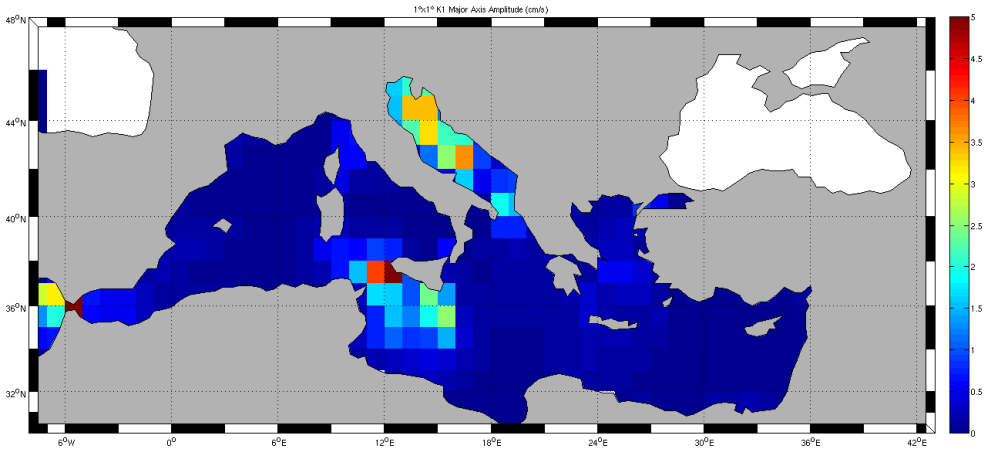
1°x1° K1 Major Axis Amplitude (cm/s)
48°N
44°N
40°N
36°N
32°N
6°W
0°
6°E
12°E
18°E
24°E
30°E
36°E
42°E
5
4.5
4
3.5
3
2.5
2
1.5
1
0.5
0

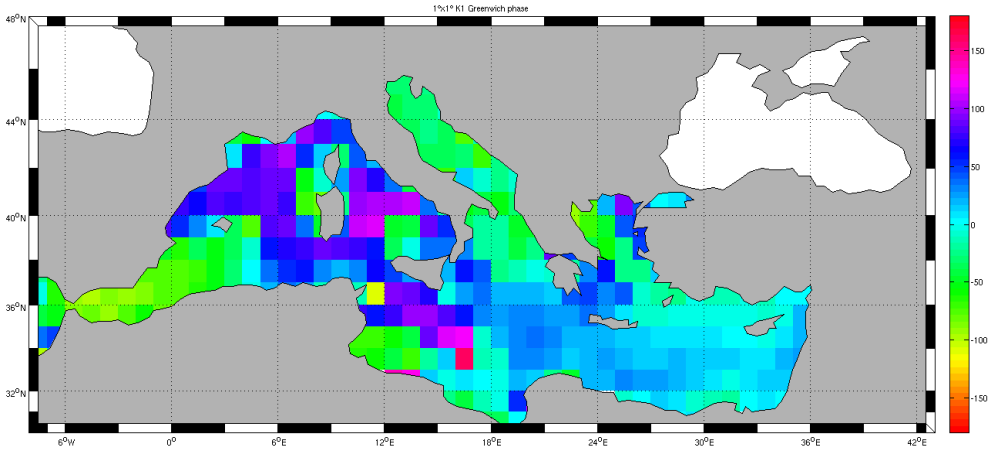
1°x1° K1 Greenwich phase
48°N
44°N
40°N
36°N
32°N
6°W
0°
6°E
12°E
18°E
24°E
30°E
36°E
42°E
150
100
50
0
-50
-100
-150

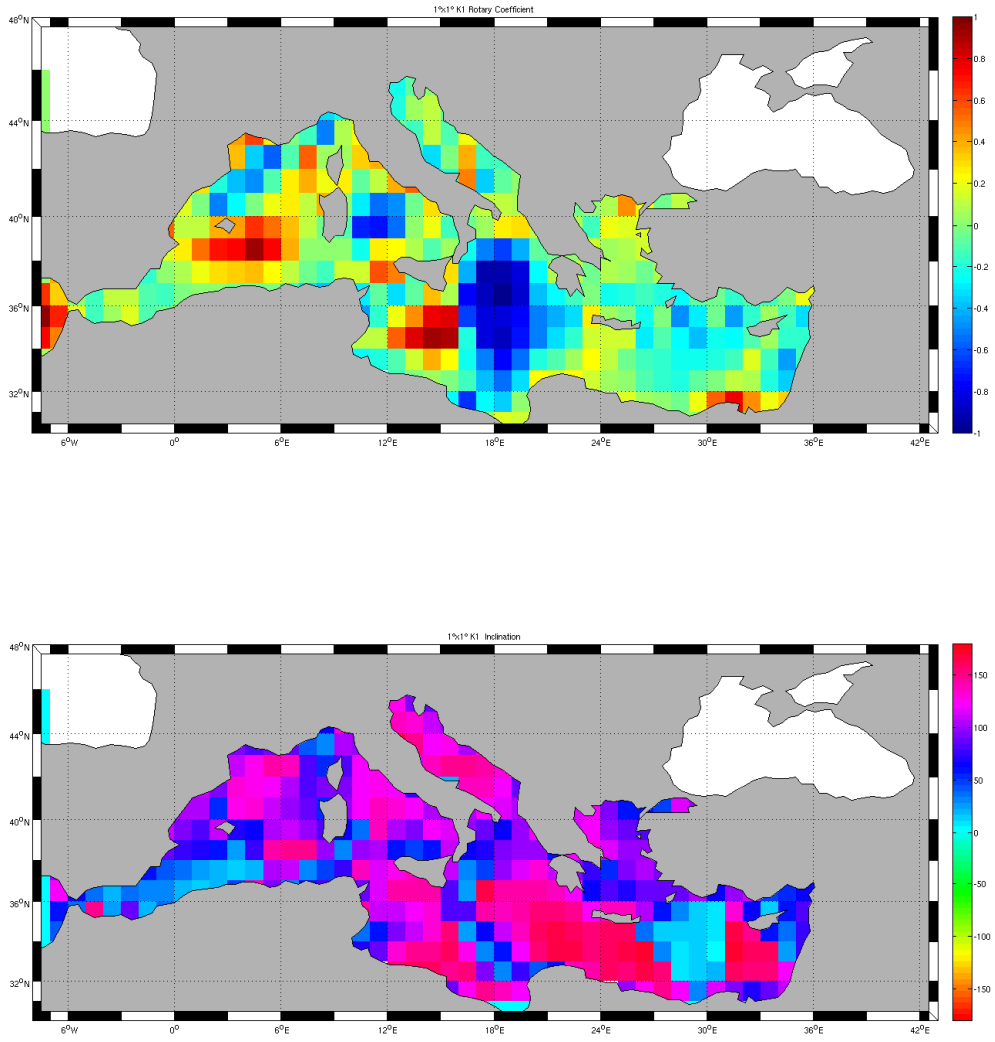

Figure 13. Same as in Figure 9 but for K1 tidal currents. Maximal amplitude of 6 cm/s occurs in the Sicily Channel.

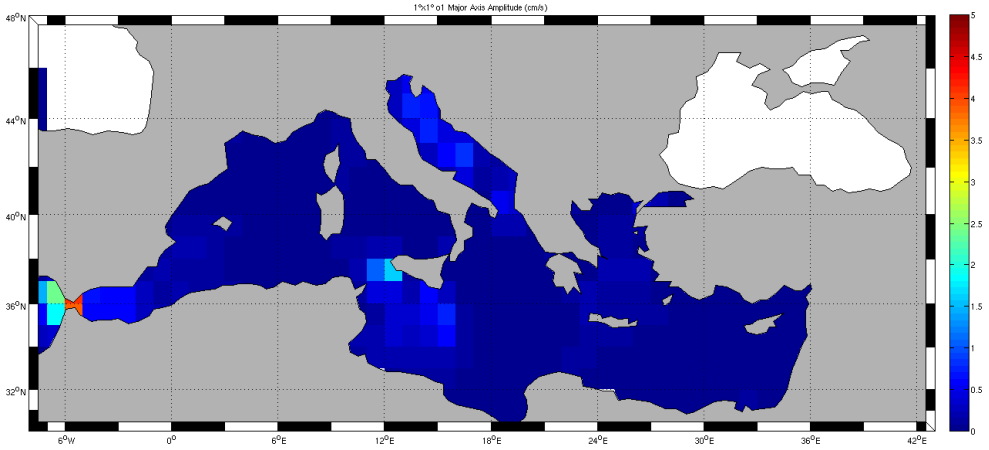
1%x1°o1 Major Axis Amplitude (cm/s)
48°N
44°N
40°N
36°N
32°N
6°W
0°
6°E
12°E
18°E
24°E
30°E
36°E
42°E
5
4.5
4
3.5
3
2.5
2
1.5
1
0.5
0

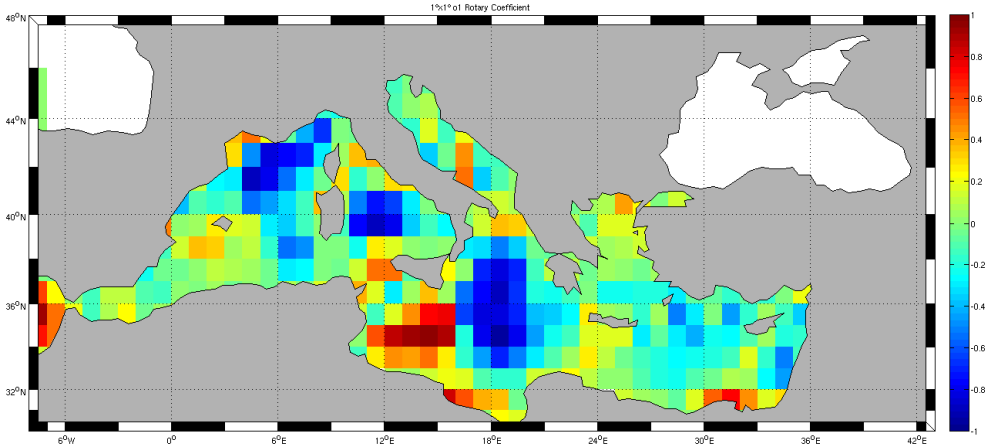
1%x1°o1 Rotary Coefficient
48°N
44°N
40°N
36°N
32°N
6°W
0°
6°E
12°E
18°E
24°E
30°E
36°E
42°E
1
0.8
0.6
0.4
0.2
0
-0.2
-0.4
-0.6
-0.8
-1

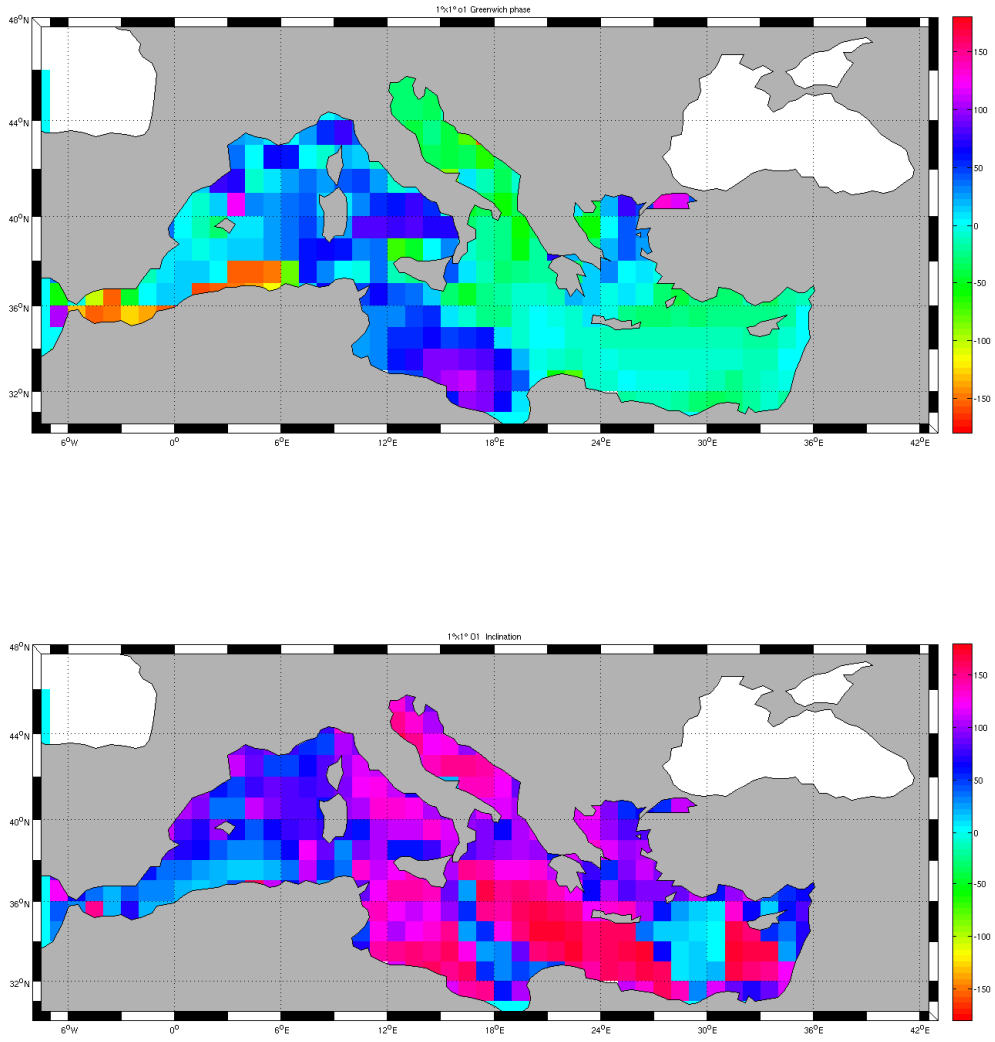

Figure 14. Same as in Figure 9 but for O1 tidal currents. Maximal amplitude of 4 cm/s occurs near the Strait of Gibraltar.

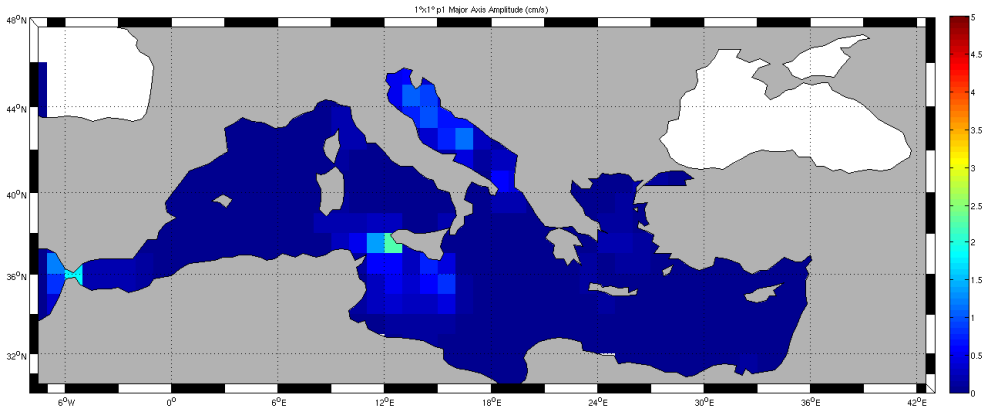
1°x1° p1 Major Axis Amplitude (cm/s)
48°N
44°N
40°N
36°N
32°N
6°W
0°
6°E
12°E
18°E
24°E
30°E
36°E
42°E
5
4.5
4
3.5
3
2.5
2
1.5
1
0.5
0

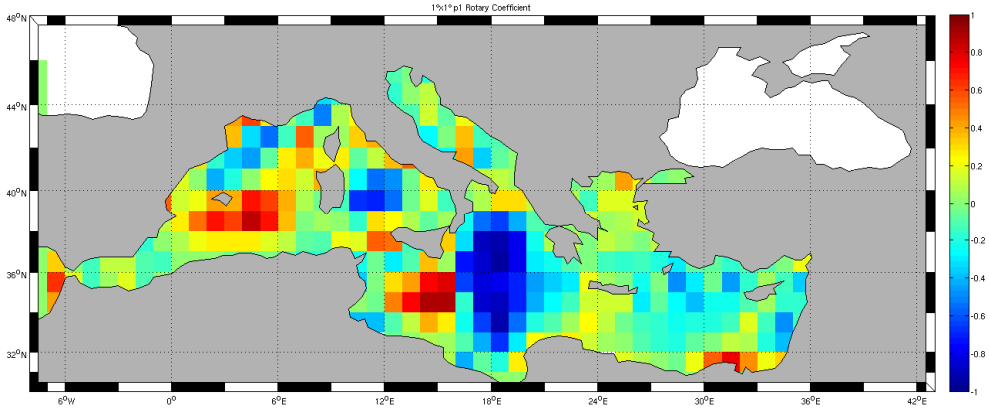
1°x1° p1 Rotary Coefficient
48°N
44°N
40°N
36°N
32°N
6°W
0°
6°E
12°E
18°E
24°E
30°E
36°E
42°E
1
0.8
0.6
0.4
0.2
0
-0.2
-0.4
-0.6
-0.8
-1

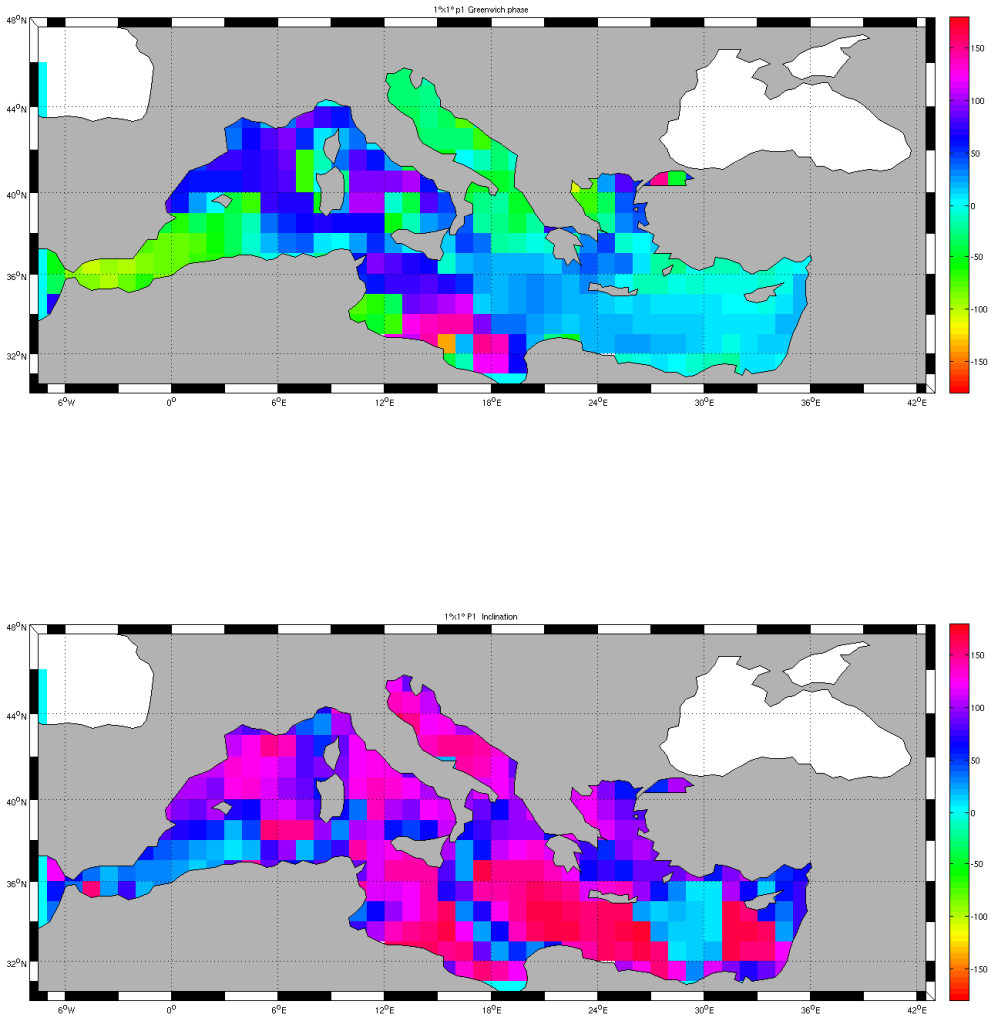

Figure 15. Same as in Figure 9 but for P1 tidal currents. Maximal amplitude of 2 cm/s occurs in the Sicily Channel.

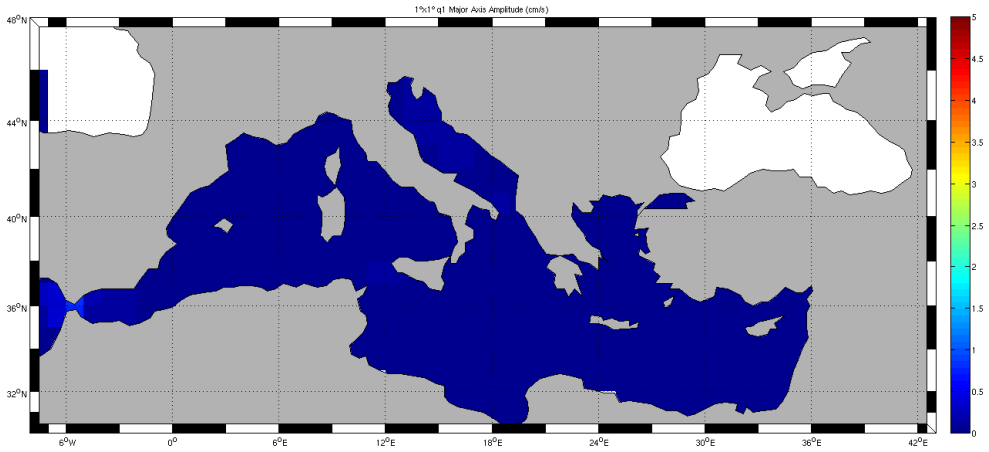
1°x1° q1 Major Axis Amplitude (cm/s)
46°N
44°N
40°N
36°N
32°N
6°W
0°
6°E
12°E
18°E
24°E
30°E
36°E
42°E
5
4.5
4
3.5
3
2.5
2
1.5
1
0.5
0

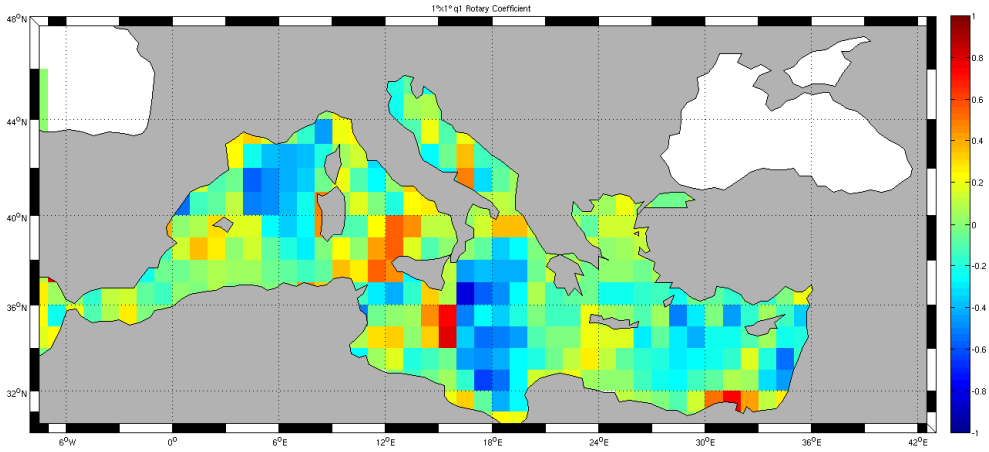
1°x1° q1 Rotary Coefficient
46°N
44°N
40°N
36°N
32°N
6°W
0°
6°E
12°E
18°E
24°E
30°E
36°E
42°E
1
0.8
0.6
0.4
0.2
0
-0.2
-0.4
-0.6
-0.8
-1

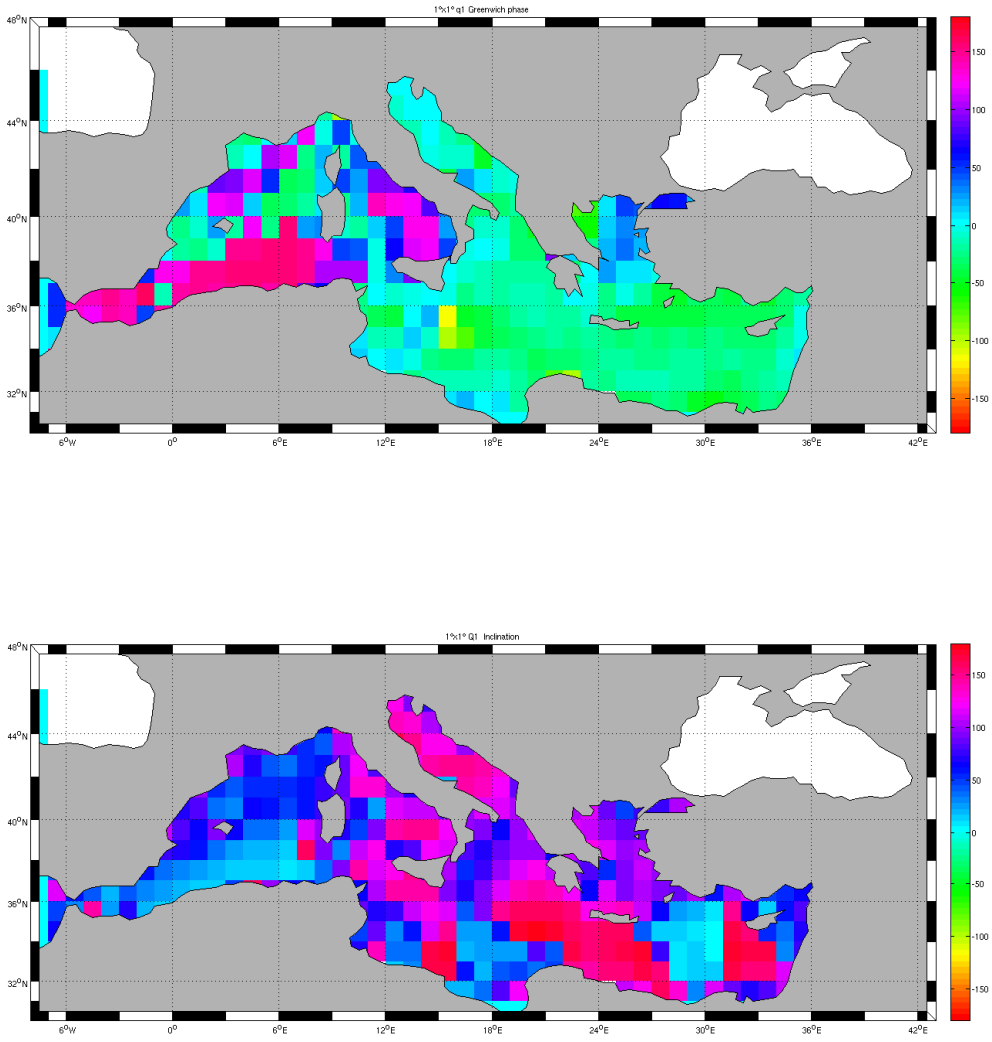

Figure 16. Same as in Figure 9 but for Q1 tidal currents.

5. Conclusions

For the World Ocean, the TPXO7.2 model simulates tidal currents whose amplitude can reach about 1 m/s in shallow marginal seas or coastal areas (see M2 currents in Yellow Sea). The M2 constituent is the most important and its amplitude is correlated with the bottom topography of the deep ocean (Fig. 1). The second most important constituent is K1 (with amplitude reaching about 60 cm/s in Ross Sea). It appears less influenced by the bottom topography in the deep open ocean.

6. References

Egbert, G. D., A. F. Bennett, and M. G. G. Foreman (1994). TOPEX/POSEIDON tides estimated using a global inverse model, J. Geophys. Res., 99(C12), 24821–24852, doi:10.1029/94JC01894.

Egbert, G. D. and S. Y. Erofeeva (2002). Efficient Inverse Modeling of Barotropic Ocean Tides. J. Atmos. Oceanic Technol., 19, 183–204.
doi: http://dx.doi.org/10.1175/1520-0426(2002)019<0183:EIMOBO>2.0.CO;2

Egbert, G. D. And R. D. Ray (2003). Semi-diurnal and diurnal tidal dissipation from TOPEX/Poseidon altimetry. Geophys. Res. Letters, 30(17), doi: 10.1029/2003GL017676.

Kantha, L.H. (1995). Barotropic tides in the global oceans from a nonlinear tidal model assimilating altimetric tides: 1. Model description and results. Journal of Geophysical Research 100: doi: 10.1029/95JC02578

Ray, R., D (2001). Inversion of oceanic tidal currents from measured elevations. Journal of Marine Systems, 28, 1–18.

Stammer, D., et al. (2014). Accuracy assessment of global barotropic ocean tide models, Rev. Geophys., 52, 243–282, *doi:*10.1002/2014RG000450